Molecular dynamics study of the thermal and the density effects on the local and the large-scale motion of polymer melts: Scaling properties and dielectric relaxation

A. Barbieri, E. Campani, S. Capaccioli, and D. Leporini[a)]
Dipartimento di Fisica "Enrico Fermi," Università di Pisa, via F. Buonarroti 2, I-56127 Pisa, Italy and INFM Unità di Ricerca di Pisa

(Received 5 September 2003; accepted 7 October 2003)

Results from a molecular dynamics simulation of a melt of unentangled polymers are presented. The translational motion, the large-scale and the local reorientation processes of the chains, as well as their relations with the so-called ''normal'' and ''segmental'' dielectric relaxation modes are thoroughly investigated in wide temperature and pressure ranges. The thermodynamic states are well fitted by the phenomenological Tait equation of state. A global time-temperature-pressure superposition principle of both the translational and the rotational dynamics is evidenced. The scaling is more robust than the usual Rouse model. The latter provides insight but accurate comparison with the simulation calls for modifications to account for both the local chain stiffness and the nonexponential relaxation. The study addresses the issue whether the temperature or the density is a dominant control parameter of the dynamics or the two quantities give rise to comparable effects. By examining the ratio $|\alpha_\tau|/\alpha_P$ between the isochronic and isobaric expansivities, one finds that the temperature is dominant when the dynamics is fast. If the relaxation slows down, the fluctuations of the free volume increase their role and become comparable to those of the thermal energy. Detectable cross-correlation between the ''normal-mode'' and the ''segmental'' dielectric relaxations is found and contrasted with the usual assumption of independent modes. © *2004 American Institute of Physics.* [DOI: 10.1063/1.1630293]

I. INTRODUCTION

Although a number of different experimental techniques (such as dielectric and mechanical spectroscopies, EPR and NMR, light and neutron scattering, etc.) are available to probe the relaxation properties of polymers and glass-forming liquids over a broad range of time scales, a complete understanding of the relaxation dynamics is still far to be achieved.[1–4] Nonetheless, the experiments unambiguously evidence the huge increase of the structural relaxation time with a super-Arrhenius temperature behavior near the glass transition temperature T_g. In order to explain these results, a variety of theoretical models have been proposed in the past. Some of them aimed at establishing the relationship between the dynamics and the thermodynamic properties near the glass transition (time scale: $10^{-5}-10^{2}$ s);[5,6] others found that a well-defined crossover to the characteristic dynamics leading the system to the structural arrest is located at temperatures which are higher than T_g.[7]

The pioneering studies of Williams,[8] Sasabe and Saito[9] and Johari and Whalley[10] have earlier pointed out that a deeper insight into the dynamics of glass-forming liquids and amorphous polymers is gained by the knowledge of the relaxation times as a function of both temperature and pressure. In fact, the possibility to reach the glassy state by two alternative paths, i.e., by cooling or compressing, enables a more stringent test of several theories, which usually predict a Vogel–Fulcher kind of behavior for the temperature dependence of the relaxation time but different pressure dependencies. In the last decade, this remark motivated several investigations of the dynamics of low-molecular-weight and polymeric glass formers as a function of both the temperature and the pressure by using various experimental techniques.[11–14] Failures of some models in describing the isothermal data under variable pressure[15] as well as strikingly good agreement with the predictions of other models for both isothermal and isobaric data[16–20] were reported. The above studies pointed out that the key feature of the models is the different relevance which is given to the available free volume and the activated jumps to account for the diffusion in the supercooled state. In fact, as temperature is lowered, the molecular motions become more restricted, due to both the decrease of the thermal energy and the increased molecular packing.[21,22] If the dynamics near the glass transition appears to be obviously affected by both thermal and density effects, it is still a matter of wide debate which one (decreasing volume, decreasing temperature, or both) plays the major role on approaching the glass transition.[21–23] The solution of this problem is of fundamental importance for the complete understanding of the glass transition. Recently, from high-pressure viscosity data for triphenyl-phosphite and glycerol, Ferrer *et al.*[23] concluded that the temperature rather than the density sets the super-Arrhenius behavior close to T_g at atmospheric pressure and that the lack of free volume leads to negligible effects, except maybe at very high pressures. On the other hand, Ngai *et al.*[24] more recently found that the

a)Electronic mail: dino.leporini@df.unipi.it

thermal variations of unoccupied volume of various glass formers, measured by positronium annihilation lifetime spectroscopy, reflect changes in the dielectric α-relaxation time over a wide temperature range, implying that the free volume cannot be neglected in analyzing the structural relaxation properties. Moreover, the latest studies by Paluch and coworkers assessed the volume dependence of the structural relaxation time of glass-forming liquids near the glass transition by using combined temperature and pressure variations.[25–27] They evidenced that fluctuations in both the thermal energy and the free volume contribute to the dynamics of supercooled liquids. Volume considerably influences the supercooled dynamics of low-molecular-mass van der Waals liquids at ambient pressure,[25] while it seems less important, or at least comparable, to temperature in driving the dynamics at higher pressures or in polymeric systems.[25,28] The role of the volume becomes negligible compared to the thermally activated process in hydrogen-bonded systems.[23]

The above survey of the experimental results shows that the microscopic dynamics close to the glass transition is in principle affected by both the activated processes and the available free volume. This feature suggests further theoretical work to combine these mechanisms, e.g., by relating the heights of the potential energy barriers and the local density.

Experiments on polymeric melts at high pressure have been recently performed by means of dielectric,[29,30] heat capacity,[31] and photon correlation spectroscopy.[32] The activation volume was found to increase at higher pressure. The studies evidenced that the relaxation process functions do not change appreciably with the pressure and the temperature, thus allowing the scaling of the data on proper master curves. The scaling factors differ for the various process and the dielectric segmental relaxation process shows a stronger pressure dependence than the normal-mode process.

A thorough analysis of the relaxation behavior of an atomistic model of the polymeric melts by changing both the pressure and the temperature is a challenging task since the intramolecular and intermolecular potentials lead to motions occurring on a wide range of time scales. To alleviate the problem and consider only the relevant degrees of freedom of the polymeric chains a number of coarse-graining strategies have been developed.[33] The bead-spring model[34–36] is a well-known scheme to replace groups of atoms of the chain by one super-atom, the bead (see Ref. 37 for a recent review). Intramolecular (''bonded'') beads are linked by quasielastic forces. Intermolecular (''nonbonded'') beads interact via analytical potentials, e.g., the Lennard–Jones potential. Bennemann *et al.* carried out a recent molecular dynamics (MD) study of polymer melts by the bead-spring model at different pressures and temperatures and reported master curves for the incoherent intermediate dynamic structure factor evaluated at $q \simeq 2\pi/b$, being b the bond length, and the average bond orientational correlation function with rank $l=2$.[38] Kaznessis *et al.* used the bead-spring model to investigate the dielectric relaxation of concentrated polymer solutions.[39] They evidenced that the presence of dipoles did not influence the static and dynamic properties of the chains in any significant fashion. Therefore, the dielectric permittivity was derived by dropping the charges and by using only equilibrium simulations, instead of resorting to more elaborate approaches requiring the evaluation of the nonequilibrium response of charged polymer to the presence of external time-dependent electric fields. The findings of Kaznessis *et al.* parallel well-known experimental evidences that in most polymers, e.g., polyisoprene, the dipole moment is small and the intermolecular and intramolecular dipole–dipole interactions are negligible.[40]

TABLE I. Points in the (P,T) plane investigated by the present study.

		Temperature							
		0.7	0.75	0.8	1.0	1.2	1.4	1.6	1.8
Pressure	0.1	•		•	•	•	•		
	0.93	•		•	•		•		•
	2.0	•	•	•	•	•	•	•	•
	3.0			•	•		•		
	4.0				•				

The system under investigation in the present article is a melt of fully-flexible, freely-jointed polymer chains being described by a bead-rod model (i.e., the springs of the bonded beads are stiff).[36,37] The study is carried out by equilibrium MD simulations and is primarily focussed on the large-scale and the local rotational dynamics with an emphasis on the dielectric properties. We follow the approach of Kaznessis *et al.*[39] and assume that ''ghost'' (i.e., noninteracting) electric dipoles are stuck into the chain with fixed geometries accounting for both the so-called normal (dipole parallel to the chain) and the segmental (dipole perpendicular to the chain) relaxation modes of type-A polymers according to the definition of Stockmayer.[41] To discriminate between the role played by the temperature and the density to set the relaxation rates, several isobaric and isothermal lines are explored.

The article is organized as follows. In Sec. II, the technical details of the simulation are given. In Sec. III, the results are discussed. They include both the static and the dynamic properties of the model system. The main conclusions are summarized in Sec. IV.

II. DETAILS OF THE SIMULATION

We investigate a system of $N=200$ fully flexible linear chains with $M=10$ monomers (beads) each. The sample is confined into a cubic box with periodic boundary conditions.

The interaction between nonbonded monomers occurs via the standard Lennard–Jones (LJ) potential

$$U(r)=4\epsilon[(\sigma/r)^{12}-(\sigma/r)^{6}]+U_{\mathrm{cut}}. \tag{1}$$

The potential is cut off at $r_{\mathrm{cut}}=2.5\sigma$ and properly shifted by U_{cut} so as to vanish at that point and to make it continuous everywhere.

To handle the boundary conditions, the minimum image convention is adopted. Neighboring monomers in the same chain are constrained to a distance $b=0.97\sigma$ by using the *RATTLE* algorithm.[42] From now on LJ units are adopted with the Boltzmann constant $k_{\mathrm{B}}=1$.

The system is studied at several pressures P and temperatures T; the values are listed in Table I. Each entry con-

sists of ten independent runs at least.

The samples are equilibrated under Nosé–Andersen[43,44] dynamics at the prescribed temperature and pressure until the average displacement of the chains' centers of mass is as large as twice the mean end–to–end distance. Data are collected during production runs in microcanonical conditions, by using a Verlet algorithm in velocity form. The time steps adopted were in the range $10^{-3} \leqslant \Delta t \leqslant 3\times 10^{-3}$, increasing with temperature, and the energy fluctuations in each run were of order $\Delta E/E \sim 10^{-4}$. No adjustment of the temperature, e.g., by rescaling the velocities, was needed during the run.

III. RESULTS AND DISCUSSION

A. Static properties

In the thermodynamic region under study the density ρ changes by about 20% ($0.8<\rho<1.05$), but the different packings affect the chain conformations in a limited way (see Fig. 10). Both the mean squared end–to–end distance $R_{ee}^2 \sim 12.0$ and the mean squared gyration radius $R_G^2 \sim 2.0$ vary by less than 5%. The stiffness of the chain is quantified by the characteristic ratio C_M which is defined as

$$C_M = R_{ee}^2/b^2(M-1). \tag{2}$$

At $T=1.4$, $P=0.93$, and $C_{10}=1.42$. Under similar thermodynamic conditions Bennemann *et al.* found $C_{10}=1.52$.[45]

The structural changes in the (P,T) region of interest are investigated in more detail in Fig. 1, which plots the radial distributions functions of the monomers $g_{\mathrm{mon}}(r)$ and of the centers of mass $g_{\mathrm{cm}}(r)$, as well as the chain structure factor $S_{\mathrm{chain}}(q)$, defined as

$$S_{\mathrm{chain}}(q) = \frac{1}{NM}\sum_{n=1}^{N}\sum_{m,m'=1}^{M}\left\langle \frac{\sin(q|\mathbf{r}_{m,n}-\mathbf{r}_{m',n}|)}{q|\mathbf{r}_{m,n}-\mathbf{r}_{m',n}|}\right\rangle. \tag{3}$$

$\mathbf{r}_{m,n}$ and the angular brackets denote the position of the m-th monomer in the n-th chain and the ensemble average, respectively. Panels (a) and (b) in Fig. 1 show the limited influence of P and T on $S_{\mathrm{chain}}(q)$ and on the average monomer radial distribution function $g_{\mathrm{mon}}(r)$. $g_{\mathrm{mon}}(r)$ exhibits more structure at lower temperature and higher pressure with small shifts of the peaks (the delta-like contribution due to adjacent monomers along the chains has been removed). No relevant changes are also seen in the radial distribution function of the center of mass $g_{\mathrm{cm}}(r)$, plotted in Fig. 1(c), which evidences the softness of the polymer coil with gyration radius R_G. The topic has been recently discussed by Guenza who presented results for $g_{\mathrm{cm}}(r)$ of unentangled chains.[46]

To characterize the so-called ''segmental'' polymer dynamics it is useful to define a ''transverse'' vector $\mathbf{T}_n$ attached to the n-th molecule as follows:[47]

$$\mathbf{T}_n = \sum_{m=2}^{M-1} \mathbf{t}_{m,n} \tag{4}$$

with

$$\mathbf{t}_{m,n} = (-1)^m(\mathbf{b}_{m-1,n}-\mathbf{b}_{m,n}), \tag{5}$$

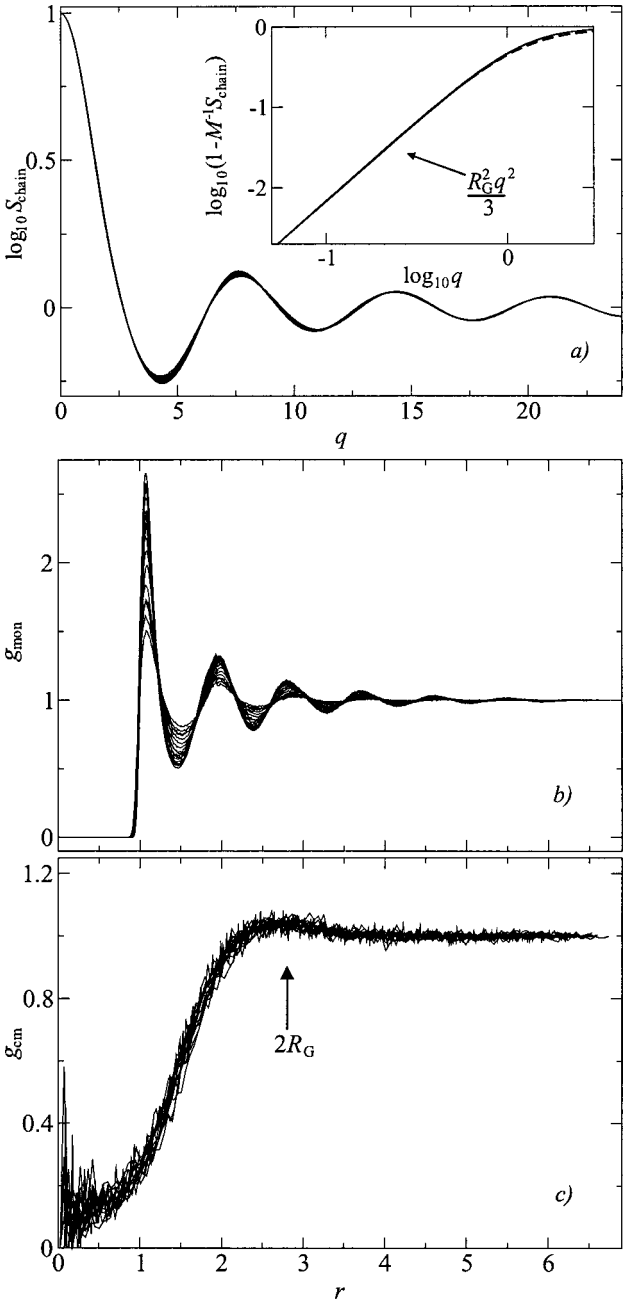

FIG. 1. (a) Chain structure factor, (b) radial distribution functions of the monomers, and (c) radial distribution functions of the centers of mass for all the investigated temperatures and pressures. The inset compares $S_{\mathrm{chain}}(q)$ in the region $q \leqslant 2\pi/R_{ee}$ with the low-q expansion for a discrete Gaussian chain (dashed line).

where $\mathbf{b}_{m,n}$ is the unit vector along the m-th bond of the the n-th chain

$$\mathbf{b}_{m,n} = \frac{1}{b}(\mathbf{r}_{m,n}-\mathbf{r}_{m+1,n}). \tag{6}$$

The vector $\mathbf{t}_{m,n}$ is locally orthogonal to the chain backbone

$$\mathbf{t}_{m,n}\cdot(\mathbf{r}_{m-1,n}-\mathbf{r}_{m+1,n}) = 0 \quad (1<m<M). \tag{7}$$

The mean squared magnitude of the vector $\mathbf{T}_n$ will be denoted by $T_\perp^2$.

Figure 2(a) shows the dependence of R_{ee}^2 and $T_\perp^2$ on the density ρ. A correlation is evident, as well as a definite trend

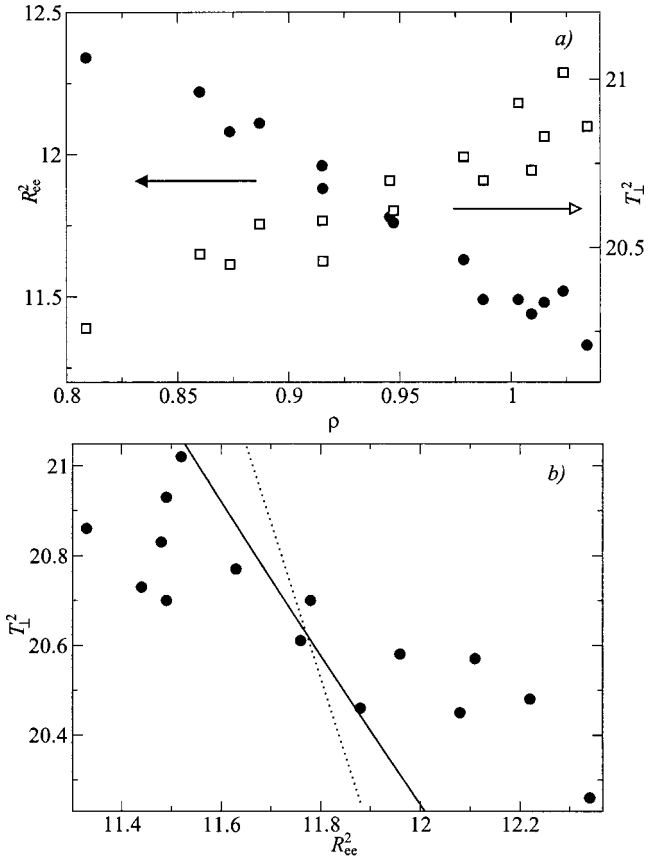

FIG. 2. (a) Density dependence of R^2_{ee} (black symbols, left axis) and $T^2_\perp$ (open symbols, right axis) for all the simulated (P,T) pairs and (b) best-fit of $T^2_\perp$ vs R^2_{ee} (symbols) with the linear law derived by combining Eqs. (9) and (12) with $b=1.01$ (dotted line). The continuous line is a fit with Eq. (13) with $b=0.94$. The actual bond size is $b=0.97$.

versus density: the denser the system, the smaller the value of R^2_{ee} and the larger that of $T^2_\perp$. Hence, there is a slight shrinking of the chains due to the non-bonded interactions.[45]

By standard algebra one finds that

$$R^2_{ee}=(M-1)b^2[1+(M-2)\cos\tilde{\theta}] \tag{8}$$

$$\simeq(M-1)b^2+2(M-2)b^2\cos\hat{\theta}, \tag{9}$$

where

$$\cos\tilde{\theta}=\frac{1}{N(M-1)(M-2)}\sum_{n=1}^{N}\sum_{m'\neq m=1}^{M-1}\langle\mathbf{b}_{m,n}\cdot\mathbf{b}_{m',n}\rangle \tag{10}$$

$$\cos\hat{\theta}=\frac{1}{N(M-2)}\sum_{n=1}^{N}\sum_{m=2}^{M-1}\langle\mathbf{b}_{m-1,n}\cdot\mathbf{b}_{m,n}\rangle. \tag{11}$$

Eq. (9) is derived by neglecting the correlations between noncontiguous bonds. Under the same approximation one finds

$$T^2_\perp\simeq 4M-10-8(M-3)\cos\hat{\theta}. \tag{12}$$

By combining Eqs. (9) and (12), a simple linear dependence between $T^2_\perp$ and R^2_{ee} is found. Figure 2(b) compares this elementary result with the numerical results. Better agreement is provided by the freely rotating model where the n-th bond is connected to the $(n+1)$-th bond with a fixed angle.[35] The model is worked out analytically and yields the following relation between $T^2_\perp$ and R^2_{ee}:

$$T^2_\perp=2\left(\frac{2b^2(M-1)}{R^2_{ee}+b^2(M-1)}\right)\times\left[(M-2)+(M-3)\frac{b^2(M-1)}{R^2_{ee}}\right]. \tag{13}$$

The fit is slightly improved [Fig. 2(b)] but the agreement is still limited by the roughness of the model.

A systematic study of the static intramolecular properties of a bead-spring polymeric system with different excluded monomeric volumes and bond lengths can be found in Refs. 48 and 49.

B. Scaling of the translational dynamics

The mean squared displacements of the terminal and central monomers and of the centers of mass are defined as

$$g_1(t)=\frac{1}{2N}\sum_{n=1}^{N}\langle|\Delta\mathbf{r}_{n,M/2}(t)|^2+|\Delta\mathbf{r}_{n,M/2+1}(t)|^2\rangle, \tag{14}$$

$$g_3(t)=\frac{1}{N}\sum_{n=1}^{N}\langle|\Delta\mathbf{r}_n^{(\mathrm{cm})}(t)|^2\rangle, \tag{15}$$

$$g_4(t)=\frac{1}{2N}\sum_{n=1}^{N}\langle|\Delta\mathbf{r}_{n,1}(t)|^2+|\Delta\mathbf{r}_{n,M}(t)|^2\rangle. \tag{16}$$

Representative plots of g_1, g_3, and g_4 are shown in Fig. 3(a). Four distinct dynamical regimes are clearly seen. At short times ($t\lesssim 0.1$) the motion is ballistic: $g_i\propto t^2$. At intermediate times ($0.1\lesssim t\lesssim 5$) the monomers get trapped into the cage of nearest neighbors, resulting in a plateau-like region of the g_i; up to this time the monomers' behavior is independent on the position along the chain. Trapping exhibits marked non-Gaussian features. This is evidenced by the non-Gaussian parameter α_2 which is defined as

$$\alpha_2(t)=\frac{3}{5}\frac{\langle|\Delta\mathbf{r}(t)|^4\rangle}{\langle|\Delta\mathbf{r}(t)|^2\rangle^2}-1. \tag{17}$$

Figure 3(a) shows a typical plot of α_2. It is seen that in the cage regime α_2 is large.

Cage restructuring occurs close to the time t^* when α_2 reaches its maximum. This is similar to what happens in molecular liquids.[50] However, at $t>t^*$ molecular liquids undergo free diffusion, but in polymers the connectivity drives the motion of monomers to a subdiffusive regime, i.e., $g_i\propto t^{x_i}$ with $x_i<1$ depending on their positions along the chain: $x_1\simeq 0.62$, $x_4\simeq 0.69$. For displacements larger than R^2_{ee} the monomer motion becomes diffusive with diffusion coefficient D defined as

$$D=\lim_{t\to\infty}\frac{g_3(t)}{6t}. \tag{18}$$

At intermediate, i.e., $t>t^*$, and long times the common belief is that the finer details of the interactions between each monomer and its surroundings may be neglected and the

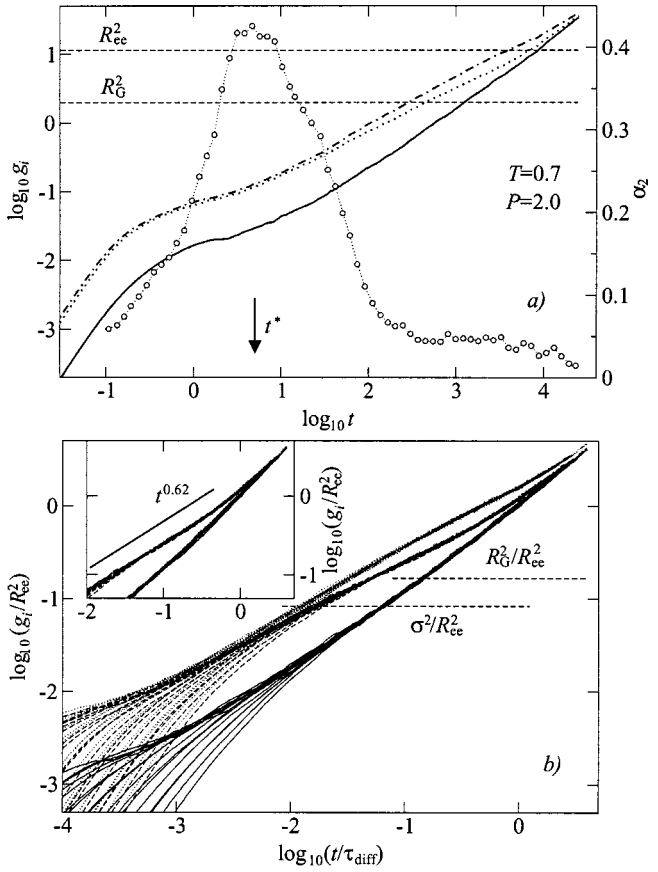

FIG. 3. (a) Mean squared displacements (left axis) of the center of mass g_3 (solid line), the central monomer g_1 (dotted line), and the terminal monomer g_4 (dot-dashed line). The open circles represent the non-Gaussian parameter α_2 (right axis), the dotted line being a guide for the eye and (b) master curves of g_1, g_3, and g_4 in units of R_{ee}^2 for all the investigated thermodynamic states. Refer to the curves of panel (a) to identify the corresponding master curves. The time is rescaled by the diffusion time τ_{diff}. The inset shows how the scaled subdiffusive regime of the central monomer merges with the scaled diffusive regime of the center of mass at long times.

motion is accounted for by average viscoelastic forces. This is a delicate point. As an example, in Sec. III C, it will be shown that the rotational correlation functions are stretched and in Sec. III H, that stiffness effects must be included to model also the relaxation of flexible chains. Both findings warn that the monomer-background interaction has nontrivial features which, expectedly, are poorly accounted for by mean-field approaches. Nonetheless, detailed information about short-range motions of the chain is customarily sacrificed to gain a tractable model for the long-range motions. The Rouse model for a melt of unentangled chains is a well-known example.[34,35] The model gives an inherently poor account of the fast and very localized motions of the chain ends whereas it predicts the subdiffusion of the inner monomers with $x_1=0.5$.[35] The larger value of x_1 is attributed to the shortness of the chain leading to an early crossover from the subdiffusive to the free diffusion regime.[45]

The viscoelastic picture of the polymer motion exhibits scaling properties. Figure 3(a) shows that the crossover between the subdiffusive and the diffusive regimes of the monomers occurs when their mean squared displacement equals R_{ee}^2. This happens at the so-called diffusion time τ_{diff}

$$\tau_{diff}=\frac{R_{ee}^2}{6D}. \tag{19}$$

Then, the two regimes must be collapsed on master curves, whose shape depends on the particular monomer, if one defines the reduced quantities g_i/R_{ee}^2 and t/τ_{diff}. It is worth noting that the scaling features are more general than the Rouse model.

Indeed, Fig. 3(b) proves the above scaling procedure for all the thermodynamic states under investigation and evidences a time-temperature-pressure superposition principle (TTPSP) when the mean squared displacements g_1, g_3, and g_4 exceed the squared bead size σ^2. Such displacements occur when the cage relaxes. In this regime the connectivity plays a role and the displacement of the central bond and the one of the terminal bond are different, the latter being larger. In particular, the scaling works nicely even for the terminal monomers whose dynamics is not well described by the Rouse model.

In Sec. III C, it will be shown that TTPSP holds for the rotational dynamics as well.

C. Scaling of the rotational dynamics

The large-scale and the local reorientation are now characterized. To this aim, the rotational correlation functions of the end–to–end vector, the ''transverse'' vector, and the different bonds of the chain are defined as

$$C_{ee}(t)=\frac{1}{NR_{ee}^2}\sum_{n=1}^{N}\langle \mathbf{R}_n(t)\cdot\mathbf{R}_n(0)\rangle, \tag{20}$$

$$C_{\perp}(t)=\frac{1}{NT_{\perp}^2}\sum_{n=1}^{N}\langle \mathbf{T}_n(t)\cdot\mathbf{T}_n(0)\rangle, \tag{21}$$

$$C_{(m,l)}(t)=\frac{1}{N}\sum_{n=1}^{N}\langle P_l[\mathbf{b}_{m,n}(t)\cdot\mathbf{b}_{m,n}(0)]\rangle, \tag{22}$$

where $P_l(x)$ is the Legendre polynomial of order l and $\mathbf{R}_n$ is the end–to–end vector of the n-th molecule. The central and the terminal bonds will receive special attention and their correlation functions will be denoted, respectively, as

$$C_{(c,l)}(t)\equiv C_{(5,l)}(t), \tag{23}$$

$$C_{(t,l)}(t)\equiv \tfrac{1}{2}[C_{(1,l)}(t)+C_{(9,l)}(t)]. \tag{24}$$

The mean rotational correlation times τ_i are also of interest. They are defined as the area below $C_i(t)$

$$\tau_i=\int_0^{\infty}C_i(t)dt. \tag{25}$$

In Fig. 4 representative plots of the above correlation functions are shown. Each correlation function exhibits different decay regimes at different times. This is emphasized by the insets of Fig. 4 which plot the data so as to convert possible stretched exponentials with stretching parameter β into straight lines with slope β. The reorientation of R_{ee} is the slowest process. The decay of $C_{ee}(t)$ is fairly well fitted across all the time window by a stretched exponential with stretching parameter $\beta=0.84$ (not shown). The other decays,

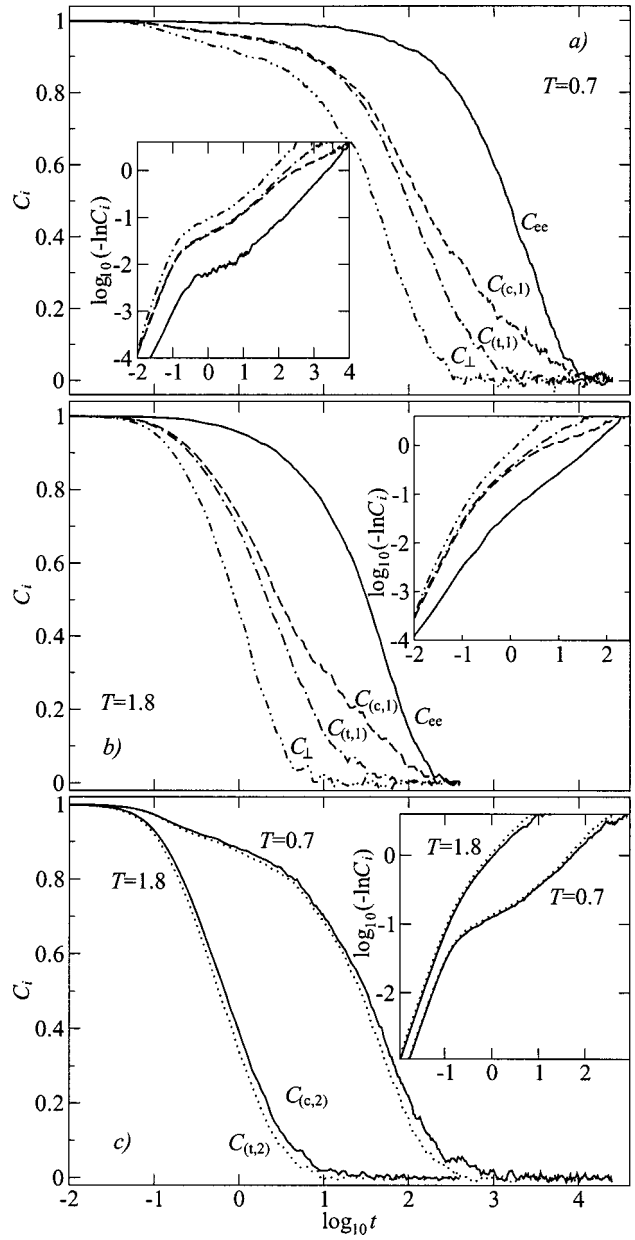

FIG. 4. (a) and (b) the rotational correlation functions for $l=1$ and (c) $l=2$ for $T=0.7$, 1.8, and $P=2.0$. The insets emphasize the different decay regimes of each correlation function. See text for details.

pertaining to local reorientation processes, are faster and not fitted by stretched exponentials. For $C_{(c,l)}(t)$, $l=1,2$ the decay is accounted for by suitable normal-mode expansions which will be discussed elsewhere.[51] Figure 4 shows that, at $T=0.7$ and $P=2.0$, $C_{(c,1)}(t)$ and $C_{(t,1)}(t)$ are virtually identical for $t\lesssim 10$ but at longer times the former decays more slowly. This is understood by referring to Fig. 3(a). It is seen that the corresponding mean square displacements $g_1(t)$ and $g_4(t)$ are coincident for $t\lesssim t^*\approx 10$ whereas the connectivity slows down the displacements of the central bond at longer times. Correlation functions with $l=2$ have faster decays and are therefore less able to discriminate between the position of the monomers. This explains why in Fig. 4 $C_{(c,l)}(t)$ and $C_{(t,l)}(t)$ with $l=2$ are closer to each other than the corresponding curves with $l=1$. The insets of Fig. 4 evidence that all the rotational correlation functions under study are affected by the trapping occurring during the cage dynamics in a small but appreciable way. The localization manifests itself as a plateau-like region located in the same time region where also the linear displacement exhibits a similar behavior (see Fig. 3). It is interesting to compare the results on the l-dependence of the rotational correlation functions of polymers with the one which is evidenced by simulations of supercooled diatomic molecules[52,53] and network-forming liquids.[54] It was found that the rotational correlation functions in the ballistic regime exhibit a larger drop on increasing l, reach a plateau-like region in the cage regime and vanish for times longer than the structural relaxation times.[52–54] As a consequence, the mean rotational correlation times become shorter on increasing l.[52–54] Similar effects on the correlation functions and the related correlation times of the central and terminal bonds are seen in Figs. 4 and 8, respectively. The plateau value in the polymer melt is higher than in diatomic molecules even if the temperature is higher[52,53] and comparable to the one observed in network-forming liquids.[54] The studies also pointed out that the rotational correlations of diatomic molecules die at $t\sim 2t^*$ for $l\leqslant 4$ at the lowest temperatures $T\sim 0.5$.[50,52] In the present case, due to the connectivity of the polymer chain, they extend for times being at least about 40 times longer than t^* even for the terminal bonds at $T=0.7$ [see Figs. 3(a) and 4].

The scaling properties of the displacement which were discussed in Sec. III B suggest that the reorientation process may exhibit the same feature too. To this aim the reduced time $t/\overline{\tau}$ is defined, $\overline{\tau}$ being the time where $C_{ee}(\overline{\tau})=1/e$. Over all the thermodynamic region under investigation it is found that the ratio $\tau_{diff}/\overline{\tau}=3.40\pm 0.18$ (see below, Fig. 8). The Rouse model predicts $\tau_{diff}/\overline{\tau}=\pi^4/24\simeq 4.06$.[34,35]

First, we test the scaling for one selected isobar and one selected isotherm. Figures 5 and 6 show the resulting master curves proving that the scaling works at long times, i.e., $t>t^*$, for all the rotational correlation functions. The scaling is lost at short times. This was already found by simulations of supercooled diatomic molecules[52,53] and network-forming liquids.[54] Figure 7 plots the master curves of all the rotational correlation functions of the polymer melt for the thermodynamic states listed in Table I. We also plot the rotational correlation function C_{tot} which is of interest for the dielectric spectroscopy and will be defined and discussed in Sec. III G. Together with the findings of Sec. III B (see Fig. 3), Fig. 7 proves that TTPSP works in the thermodynamic region under study and that the master curves result by scaling in terms of the single time scale $\overline{\tau}$ (or equivalently τ_{diff}).

Additional evidence about the TTPSP is collected by comparing $\overline{\tau}$ with the mean rotational correlation times τ_i. Notice that $\tau_{ee}\simeq\overline{\tau}$. It is also of interest to evaluate by Eq. (25) the mean bond rotational correlation time τ_{avg} from the mean bond correlation function

$$C_{avg}(t)=\frac{1}{M-1}\sum_{m=1}^{M-1} C_{(m,1)}(t). \tag{26}$$

Figure 8 shows the dependence of the the ratios $\tau_i/\overline{\tau}$ on the density for all the (P,T) states investigated. It is seen that the ratios are constant and depend on the specific rota-

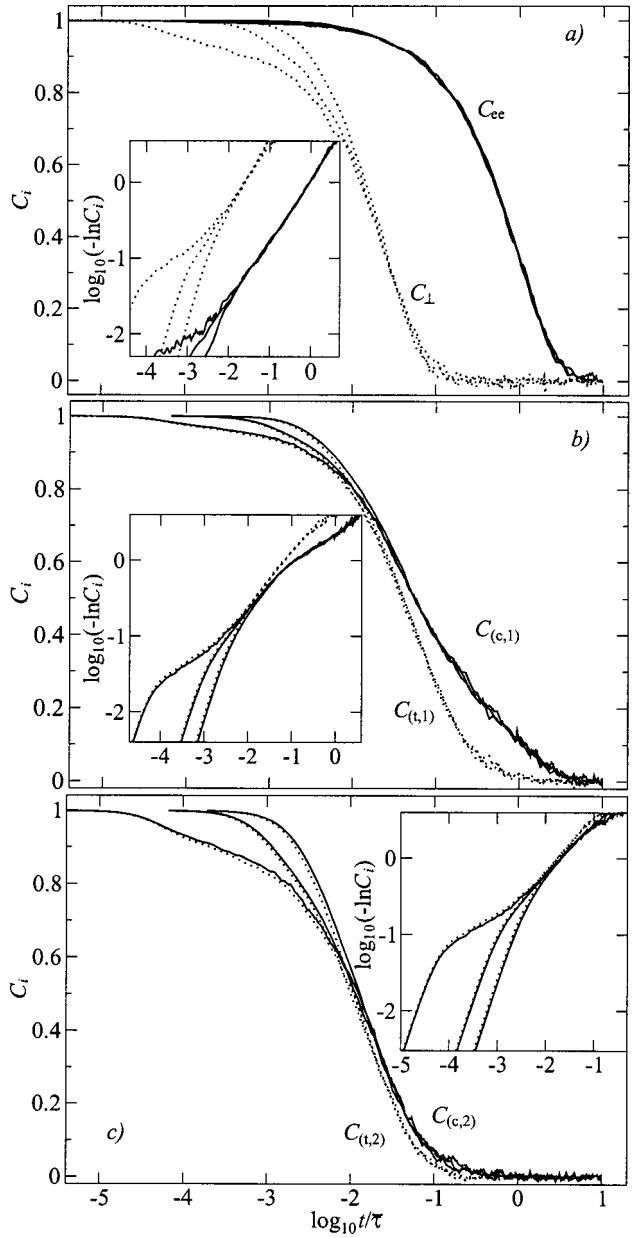

FIG. 5. Master curves of all the rotational correlation functions for the isobar $P=2.0$ and the temperatures $T=0.7$, 1.2, and 1.8. The insets emphasize the different decay regimes of each correlation function.

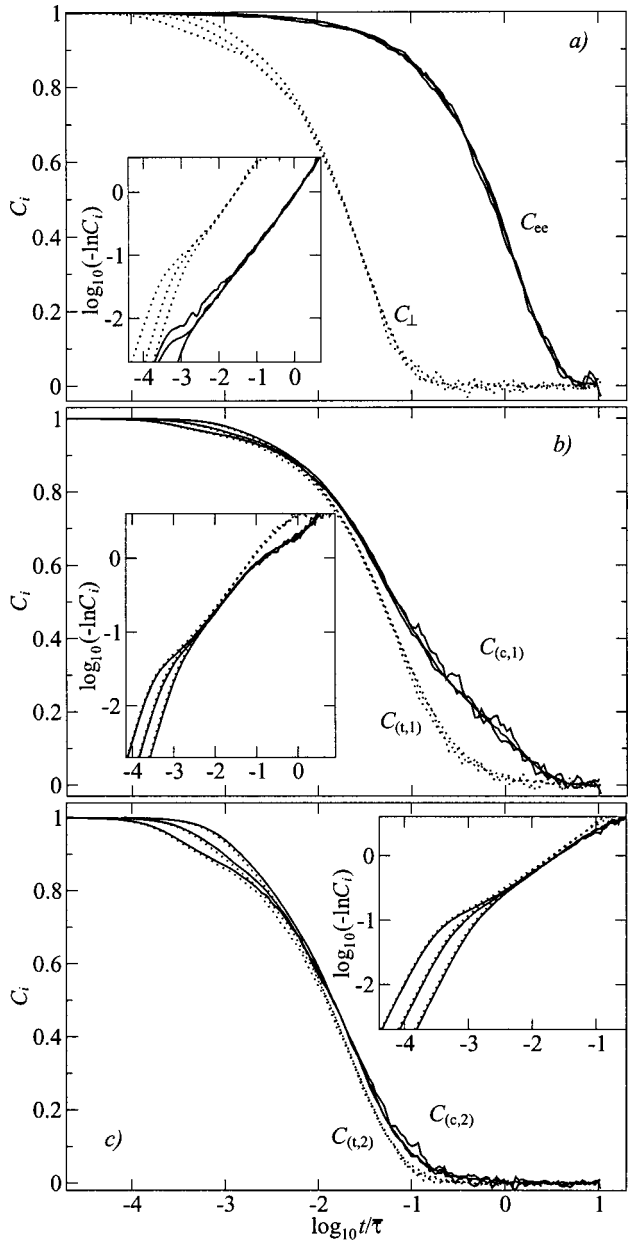

FIG. 6. Master curves of all the rotational correlation functions for the isotherm at $T=1.0$ and the pressures $P=0.1$, 2.0, and 4.0. The insets emphasize the different decay regimes of each correlation function.

tional correlation function. This finding is readily explained in that τ_i is mostly affected by the long-time decay of $C_i(t)$ which scales.

Some comments on the ratios between the rotational correlation times presented in Fig. 8 are in order.

The ratio $\tau_{ee}/\overline{\tau}$ is slightly larger than 1; this is due to the stretching of the correlation function $C_{ee}(t)$ ($\beta=0.84$). The ratio $\tau_{diff}/\overline{\tau}$ has been discussed above. The ratio $\tau_{(t,1)}/\tau_{(c,1)}<1$ is mainly due to the lower connectivity of the chain ends which have larger free volume accessible to them, with respect to that available for the other monomers, e.g., the central monomer.[47,55] τ_{avg} is comparable to $\tau_{(c,1)}$; this is due to the similar behavior of the inner bonds, which hides the effect of the ones located on the chain ends.

The ratio of the correlation times with different l ranks is also worth noting. For a melt of Lennard–Jones dimers at high temperature, τ_1/τ_l was found to be nearly equal to $l(l+1)/2$ in agreement with the diffusion model.[52] In deeply supercooled states one has $\tau_1/\tau_l \sim 1$, due to the presence of jump-like motion. For the present polymeric system, the end and the central bonds have $\tau_{(t,1)}/\tau_{(t,2)} \sim 5.7$ and $\tau_{(c,1)}/\tau_{(c,2)} \sim 9.3$, respectively. The fact that both ratios exceed the prediction of the diffusion model is to be ascribed to the higher connectivity of the bonds in the chain with respect to the bond of the dimer. The same effect with larger magnitude was seen in MD simulations of the local chain motion in amorphous polyethylene and a freely rotating chain model.[56] It was found that the rotational correlation times of a bond vector **c** defined along the chain axis have the ratio $\tau_{(\mathbf{c},l=1)}/\tau_{(\mathbf{c},l=2)} \sim 10^2$. The study also addressed the reorien-

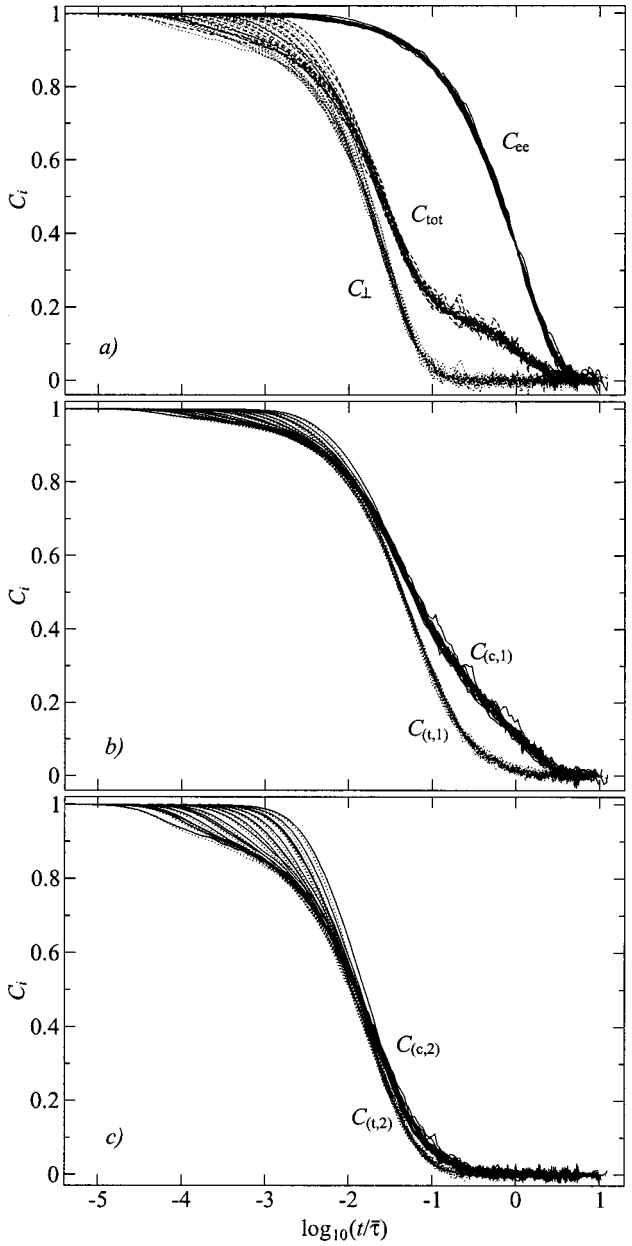

FIG. 7. Master curves of all the rotational correlation functions. The plot collects all the cases in the (P,T) region under study (see Table I). $C_{tot}(t)$ is the correlation function of the overall polarization, Eq. (38).

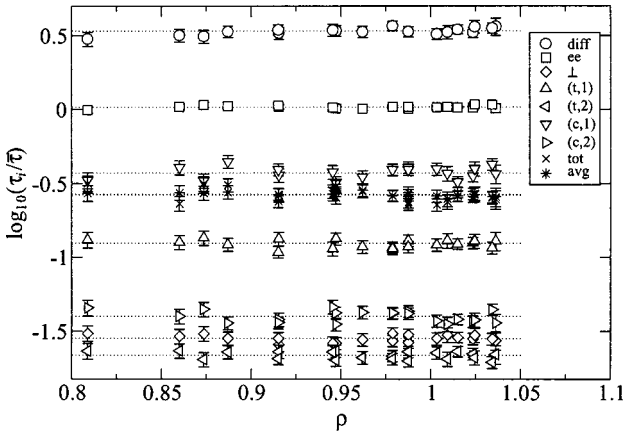

FIG. 8. Dependence of the ratios $\tau_i/\bar{\tau}$ on the density for all the simulated (P,T) states. The dotted lines are the best-fit values $\tau_{diff}/\bar{\tau}=3.40\pm0.18$, $\tau_{ee}/\bar{\tau}=1.04\pm0.03$, $\tau_{(c,1)}/\bar{\tau}=(3.7\pm0.4)\times10^{-1}$, $\tau_{avg}/\bar{\tau}=(2.7\pm0.1)\times10^{-1}$, $\tau_{tot}/\bar{\tau}=(2.6\pm0.3)\times10^{-1}$, $\tau_{(t,1)}/\bar{\tau}=(1.25\pm0.8)\times10^{-1}$, $\tau_{(c,2)}/\bar{\tau}=(4.0\pm0.4)\times10^{-2}$, $\tau_{\perp}/\bar{\tau}=(2.83\pm0.16)\times10^{-2}$, and $\tau_{(t,2)}/\bar{\tau}=(2.20\pm0.15)\times10^{-2}$.

tation of a ''bisector'' **a** and an ''out-of-plane'' **b** vector. These ''perpendicular'' vectors with respect to the chain axis exhibited faster dynamics than the bond vector **c**, $\tau_{(\mathbf{a},l=1)}\sim\tau_{(\mathbf{b},l=1)}\sim(3-5\times10^{-3})\tau_{(\mathbf{c},l=1)}$. In our case we find $\tau_{\perp}/\tau_{(c,1)}=7.6\times10^{-2}$. Hence, the relaxation of the vectors parallel to the chain axis is slower than the vectors perpendicular to it. The chain is rapidly tumbling around the chain axis or a segment of it, while this latter is slowly changing its direction following the relaxation of the local (surrounding) structure.

The anisotropy of the relaxations of the vector parallel to the chain axis and of the vectors perpendicular to it also depends on the chain properties. In our model the polymer is completely flexible because of the absence of torsional potentials and constant bond angles. This reduces the anisotropy and accounts for the lower ratios $\tau_{(m,1)}/\tau_{(m,2)}$ for $m=$c,t, and $\tau_{(c,1)}/\tau_{\perp}$ with respect to Ref. 56. The influence of the polymer structure on the anisotropy was seen in fully atomistic simulations and experiments on polyisoprene melts,[57,58] which evidenced a less pronounced anisotropy of the local motion and lower values of the ratio $\tau_{(c,1)}/\tau_{(c,2)}$ than Ref. 56. In particular, $\tau_{(c,1)}/\tau_{(c,2)}\approx6.1$ in Ref. 57, which is quite close to our result.

The results of this section extend the findings of Sec. III B and complete the evidence of the TTPSP scaling of both the translational and the rotational dynamics in the thermodynamic region under study. The scaling procedure applies to orientational correlation functions involving quite different observables (end–to–end vector, terminal and central bond, transverse vector) and different ranks of the Legendre polynomials. In Sec. III G it will be shown that it also holds true for the correlation function $C_{tot}(t)$ of interest for the dielectric relaxation which has rank $l=1$ and is affected by both the local and large-scale motion in a correlated way.

Numerical evidence of the TTPSP scaling in polymer melts was reported in Ref. 38 for chains with $M=10$ monomers, mutual Lennard–Jones interactions, and good stiffness of the bonds. It was shown that the incoherent intermediate dynamic structure factor evaluated at $q\simeq2\pi/b$, the average bond orientational correlation function, and the end–to–end correlation function (both with rank $l=2$) may be collapsed on single curves at long times. Moreover, the temperature dependence of τ_{ee} and the correlation time τ_q of the the incoherent intermediate dynamic structure factor for different q-values was plotted for different isobars. The plotted ranges were $0.45\leqslant T\leqslant1.0$ for $P=0.5$, $0.46\leqslant T\leqslant2.0$ for $P=1$, and $0.52\leqslant T\leqslant2.0$ for $P=2$. For each isobar the temperature dependence of the different correlation times was found to be rather similar even if deviations are apparent at higher temperatures for q-values larger than the maximum of the static structure factor.

Scaling is predicted by the Mode-Coupling theory[7] as well as by the Rouse model.[34,35] The Mode-Coupling theory

provided a recent microscopic justification of the Rouse model in polymer melts.[59] However, the physical basis of the scaling is rather simple in that at long times $\tau_{\rm diff}=R_{\rm ee}^2/6D$ is the only natural time scale for a melt of unentangled chains with size $R_{\rm ee}$ drifting with diffusion coefficient D. The scaling hypothesis holds across the region $t>t^*$ where the surroundings of the chain may be modeled in terms of effective, average viscoelastic forces.

The existence of a unique scaling factor well above T_g was confirmed by studies on the dynamics of polyisoprene melts performed by different experimental techniques (dielectric, time resolved and photon correlation spectroscopy, and depolarized Rayleigh and neutron scattering):[60–64] The characteristic relaxation times followed, apart from a constant factor, the same behavior with temperature. In particular, the dielectric relaxation times (rank $l=1$) related to the dipole perpendicular to the chain contour and the photocorrelation characteristic times (rank $l=2$) had a similar time scale.[64] On the other hand, recent experiments by dielectric relaxation on oligomeric and polymeric melts carried out over a wide pressure and temperature range[29–31,65] have shown that the universal scaling behavior is valid for temperatures well above T_g and breaks down in an intermediate regime still above the glass transition. MD simulations of a melt of dimers ($M=2$) also showed that τ_i (for $l=1-4$) and the rotational diffusion coefficient D_r^{-1} exhibit at intermediate temperature the same scaling law, which is lost at the lowest and the highest temperatures.[52,53]

The scaling properties depend on the length scale under investigation so the complete understanding of the above experimental and numerical results needs the clear assessment of the scales which are probed. As an example, neutron scattering evidenced that the dynamic structure factor $S(q,t)$ in polybutadiene evaluated at q-values around the maximum of the static structure factor $q_{\rm max}$ (corresponding to the interchain distance) scales with the macroscopic viscosity.[66] However, at higher q-values, e.g., the first valley of the static structure factor, a decoupling is observed at lower temperatures.[67] The q-dependence of the time-temperature superposition principle in the α-relaxation regime of a simulated polymer melt of unentangled chains has been also discussed.[68] It was found that the scaling of the coherent intermediate scattering function fails at high temperatures and high q-values ($q\sim 2q_{\rm max}$). Violations were also noticed in the early part of the decay on approaching the so-called critical temperature T_c from above.

D. Density and temperature dependence of the scaling time $\bar{\tau}$

The previous discussion proved that $\bar{\tau}$ is the relevant time scale of the present polymer model. This section presents the temperature and pressure behavior of this quantity.

The pressure dependence of $\bar{\tau}$ is shown in Fig. 9(a) for different isotherms. The curves are fitted by

$$\bar{\tau}=\bar{\tau}_{(P=0)}\exp\left(\frac{P\Delta V}{T}\right), \tag{27}$$

where ΔV is the activation volume per monomeric unit.

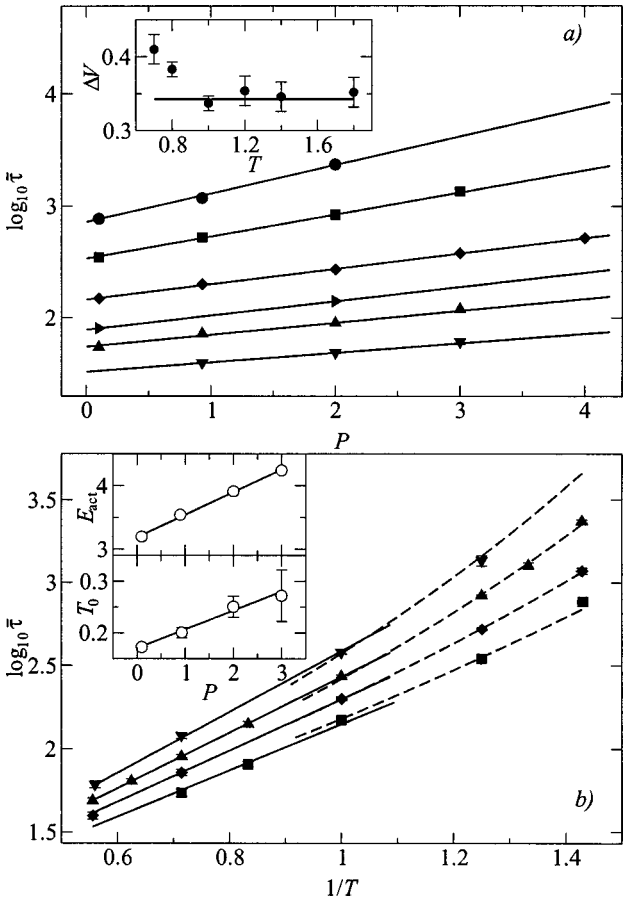

FIG. 9. The scaling time $\bar{\tau}$ versus (a) the pressure and (b) the temperature. The continuous lines in panel (a) are fits of the isotherms $T=0.7$, 0.8, 1.0, 1.2, 1.4, and 1.8 with Eq. (27). The inset plots the activation volume ΔV vs the temperature. Panel (b) plots the isobars $P=0.1$, 0.93, 2.0, and 3.0. The continuous lines are Arrhenius fits, Eq. (28). The dashed lines are VFT fits, Eq. (29). The insets show the activation energy $E_{\rm act}$ of Eq. (28) and the VFT temperature T_0 of Eq. (29).

The continuous lines in Fig. 9(a) are the best-fit curves. The inset of Fig. 9(a) shows that ΔV is constant at high temperature ($\Delta V_{HT}\simeq 0.34\pm 0.01$) and that it increases on decreasing the temperature. This behavior has been reported by several experimental[30–32,69–71] and numerical studies[72] on linear polymeric melts. At low T the increase of ΔV is believed to be reminiscent of the postulated T dependence of the cooperative volume.[30] At higher temperatures, i.e., above the critical limit for the size of cooperatively rearranging regions ΔV denotes a volume barrier. Previous experiments reported ΔV to be comparable to,[6] the monomer size few degrees above T_g, and to attain a limit of 30%–40% of the monomer size at higher temperatures.[30,31] This compares in a satisfactory way with the present work.

The temperature dependence of $\bar{\tau}$ is shown in Fig. 9(b) for different isobars. The Arrhenius law

$$\bar{\tau}=\bar{\tau}_0\exp\left(\frac{E_{\rm act}(P)}{T}\right) \tag{28}$$

does not fit the different isobars over the whole range, even if the agreement improves at higher temperatures and/or short times. A similar conclusion is drawn if one uses the Vogel–Fulcher–Tammann (VFT) equation[6,73]

$$\bar{\tau}=\bar{\tau}_{0\mathrm{VFT}}\exp\left(\frac{DT_0(P)}{T-T_0(P)}\right) \tag{29}$$

The discrepancy is expected in that it is experimentally well known that a crossover from an Arrhenius to super-Arrhenius behavior occurs several degrees above T_g.[74] This motivated us to split the whole temperature range into two intervals in order to properly account for the different dependencies. According to our data, the Arrhenius regime extends over $1\leqslant T\leqslant 1.8$ ($\bar{\tau}\leqslant 350$) whereas the VFT regime is found at $0.7\leqslant T\leqslant 1$ ($\bar{\tau}\geqslant 350$). It must be pointed out that, even if alternative functions can be employed, the VFT equation is rather adequate to fit the super-Arrhenius behavior.[72,75]

In the Arrhenius regime the attempt time was set to $\bar{\tau}_0=5.64$ for all the isobars and only the activation energy E_{act} was adjusted. The best fits are plotted in Fig. 9(b). The inset of Fig. 9(b) shows that the best-fit values of E_{act} depend linearly on the pressure P according to $E_{\mathrm{act}}=E_0+vP$ with $v=0.36\pm0.02$ and $E_0=3.20\pm0.02$, i.e., the energy barrier increases with density. The quantity v must be coincident with the high-temperature (HT) activation volume in that $\Delta V_{\mathrm{HT}}=T(\partial\ln\bar{\tau}/\partial P)=v$. In fact, the fit on the isobaric lines yields $\Delta V_{\mathrm{HT}}\simeq 0.34\pm0.01$ [see the inset of Fig. 9(a)]. The agreement is a good cross-check of the two independent fit procedures.

In the VFT regime the best-fit procedure kept fixed $\bar{\tau}_{0\mathrm{VFT}}=10.5$ and $D=11$ and adjusted only $T_0(P)$ for the different isobars. The assumption of keeping fixed $\bar{\tau}_{0\mathrm{VFT}}$ and D can be justified by the experimental evidence that, at least for moderate compression, the main influence of pressure on the VFT parameters concerns T_0, whereas $\bar{\tau}_{0\mathrm{VFT}}$ and D are virtually unchanged.[11,76–80] The best-fit results are plotted in Fig. 9(b).

The inset of Fig. 9(b) shows the linear behavior of $T_0(P)$ versus P. The linear regression $T_0(P)=T_0(0)+wP$ yields $T_0(0)=0.170\pm0.01$ and $w=(3.7\pm0.2)\times10^{-2}$. This linear dependence has been already reported in literature for polymeric melts,[30,69,79,81,82] and it is consistent, at least for moderate pressures, with both the free volume model and the Adam Gibbs model extended to deal with the density and thermal effects on the polymer dynamics.[14,16,17,78,83] A similar pressure dependence of the VFT parameters was reported in a MD simulation of polyethylene with conformational details.[72] In another MD simulation on oligomers (bead-spring model with poly-dimethylsiloxane (FENE) potential and different cut-off of the LJ potential, $M=10$) a value of $T_0(P=1)=0.34$ was found[75] which is slightly higher than the value $T_0(P=1)=0.21$ of the present study.

E. State equation

The dependence of the specific volume on T and P is plotted in Fig. 10. It is well fitted by the Tait equation, commonly used as a phenomenological equation of state of polymeric melts:[84,85]

$$V(P,T)=V(0,T)\left(1-C\ln\frac{P}{B(T)}\right),$$

$$V(0,T)=A_0+A_1T+A_2T^2, \tag{30}$$

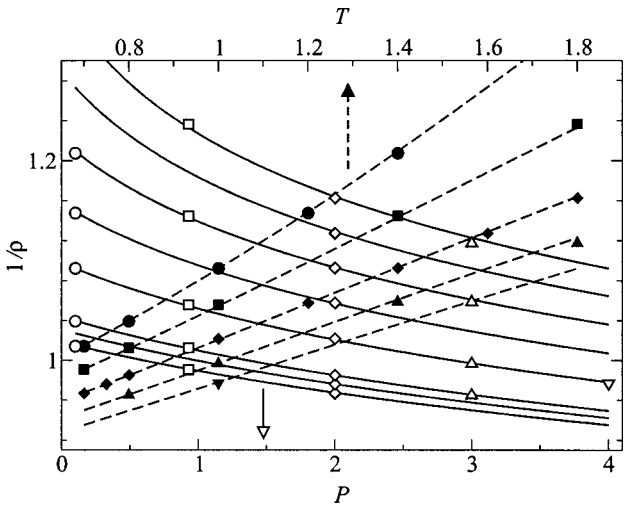

FIG. 10. Volume per monomer versus pressure (lower axis, open symbols) and temperature (upper axis, black symbols). The continuous and the dashed lines are the best-fit with the Tait Eq. (30). The parameters are $A_0=0.876\pm0.004$, $A_1=0.161\pm0.007$, $A_2=(6.1\pm0.4)\times10^{-2}$, $B_0=7.9\pm0.1$, and $B_1=1.55\pm0.04$.

$$B(T)=B_0\exp[-B_1T],$$

for real polymers $C=0.0894$.[84]

A comparison of the best-fit parameters of the present system with the ones of real polymers would be interesting. The Tait equation constrains the thermodynamic variables P and T if $V(0,T)$ and $B(T)$ are known. $B(T)$ is proportional to the isothemal bulk modulus $K(T)$ at $P=0$.

$$B(T)=CK(T), \tag{31}$$

with $K^{-1}=-V^{-1}(\partial V/\partial P)|_{P=0}$. In our model, $0.5<B(T)<2.5$ in LJ units. For real polymers far from the glassy state $B(T)\sim300$ MPa. Then, the lowest pressure under study, i.e., $P=0.1$, corresponds to pressures in the range 12–60 MPa, not far from the atmospheric pressure condition $P/B(T)<1$. The highest value $P=4.0$ is in the range of higher pressures experimentally investigated, 0.48–2.4 GPa. The conversion of $V(0,T)$ from LJ units to the real world ones would be largely arbitrary due to the highly coarse-grained picture of the polymer chain under study and will be not pursued. The lack of information prevents one to relate the temperature dependencies of $B(T)$ and $V(0,T)$. However, they may be compared by using the ratio between the fractional changes of $B(T)$ and $V(0,T)$ with the temperature, r_T, which may be expressed as

$$r_T=B_1/\alpha_{P0}, \tag{32}$$

where α_{P0} is the volume expansion coefficient at $P=0$

$$\alpha_{P0}=\frac{1}{V}\left(\frac{\partial V}{\partial T}\right)\Big|_{P=0}=\frac{A_1+2A_2T}{A_0+A_1T+A_2T^2}. \tag{33}$$

Comparing r_T as obtained from the simulation with the ones of real polymers provides a good test of the meaningfulness of using the Tait equation as fit function.

Table II lists the ratio r_T for the present model and for some selected polymers. The comparison is quite reassuring about the consistency between the thermodynamic states of

TABLE II. The dimensionless ratio $r_T = B_1/\alpha_{P0}$ for the present model and for the polymers: polybutadiene (PB), *cis*-abundance poly-isoprene (PI1), (3,4) abundance polyisoprene (PI2), poly-dimethylsiloxane (PDMS), and atactic poly-styrene (aPS).

Polymer	Ref.	M	r_T
Present work	-	10	5.55–6.41
Trans-PB	106	~2000	5.65–5.95
cis-PB	106	~2000	5.40–5.62
1,2-PB	106	~2000	6.38–6.57
PI1	106	~1500	5.96–6.31
PI2	106	~1500	6.03–6.29
PDMS	107	~13	7.37–7.64
PDMS	107	~50	6.87–6.97
PDMS	107	~80	6.75–7.05
aPS	108	-	5.75–5.85

the present coarse-grained model and those of real systems. The small discrepancies which are seen for (PDMS) deserve further work.

F. Density and thermal effects on the dynamics

The knowledge of the equation of state allows one to analyze the density dependence of the dynamics in greater detail. Figure 11 plots $\log_{10}\overline{\tau}$ versus the density for all the isobars and isotherms under investigation. Similar plots are well known from the experiments.[23,30,86] For a given density increase, the more efficient way to slow down the system is by isobaric cooling rather than by isothermal compression. In fact, by isobarically cooling a molecular liquid, both the thermal energy and the free volume available to the molecules are decreased, whereas by isothermally compressing it only the free volume changes. The finding that the density dependence of $\log_{10}\overline{\tau}$ for different isobars and isotherms does not collapse on a master curve proves that the density by itself is not the unique variable governing the dynamics. This rules out any relation between the relaxation time and the density alone, e.g., the Doolittle-like equation

$$\overline{\tau} = \tau_0 \exp\left(\frac{B}{\rho_0 - \rho}\right), \tag{34}$$

where B and ρ_0 are constant. Eq. (34) does not work also if one chooses two different sets of parameters B, ρ_0, and τ_0, one for all the isothermal paths and one for all the isobaric paths. The issue of the density scaling will be discussed more in detail in a forthcoming paper.[87]

Figure 11 prompts the question if the temperature or the density is a dominant control parameter of the dynamics or the two quantities give rise to comparable effects. The parameter of choice[23,25] to quantify the relative contributions of the temperature and the density to the dynamics along isobars is the ratio of the isobaric α_P and the isochronic α_τ expansivities to be defined as

$$\alpha_P = \frac{1}{V}\left(\frac{\partial V}{\partial T}\right)_P, \tag{35}$$

$$\alpha_\tau = \frac{1}{V}\left(\frac{\partial V}{\partial T}\right)_\tau. \tag{36}$$

If the dynamics is dominated by temperature activated processes $|\alpha_\tau|/\alpha_P$ is much larger than one, the opposite holds if the volume rules the dynamics. A ratio of order unity means that the two quantities are equally important. The inset of Fig. 11 plots the pressure dependence of $|\alpha_\tau|/\alpha_P$ for different $\overline{\tau}$. The ratio increases with the pressure at a given $\overline{\tau}$. It decreases with increasing $\overline{\tau}$ at a given pressure and reaches a limiting value at large $\overline{\tau}$. Such a behavior suggests that when the dynamics is fast (short $\overline{\tau}$) the temperature is the dominant variable. On the other hand, if the dynamics is slowed down (long $\overline{\tau}$) the available free volume becomes more important. It must be stressed that the counter-intuitive finding that the dynamics is more activated at higher pressures is supported also by experimental results,[25] and explained by the increased height of the potential energy barriers thus leading to a more activated behavior.

The ratios $|\alpha_\tau|/\alpha_P$ by the present study compare well with the experimental results: $|\alpha_\tau|/\alpha_P$ estimated for long $\overline{\tau}$ is between 0.5 and 1 for low molecular van der Waals liquids, between 1 and 2.8 for polymeric systems, and finally much higher than 1 in the very special case of hydrogen-bonded systems, following a pattern of decreasing importance of volume with respect to that of temperature activated dynamics.[23,25,28,70,88,89]

Our polymer model appears to be at the border line between polymers and van der Waals liquids, with a dynamics to which the fluctuations of the the thermal energy and the density contribute to the same extent.

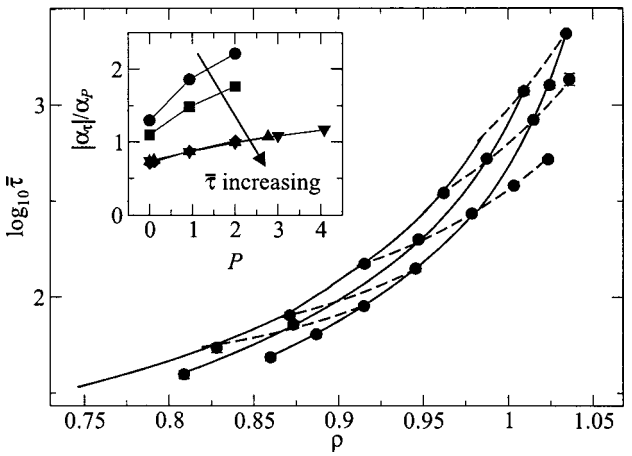

FIG. 11. Behavior of the timescale $\overline{\tau}$ vs the density along isothermal and isobaric paths. The symbols are results from the simulation, the dashed lines are the isothermal fit curves displayed in Fig. 9(a) and the continuous lines are the isobaric fit curves displayed in Fig. 9(b). The inset shows the pressure dependence of the ratio between the isobaric and isochronic expansivities. The lines correspond to $\overline{\tau}=47$ (circles), 64 (squares), 148 (diamonds), 352 (up triangles), and 524 (down triangles).

G. Dielectric relaxation of type-A polymers: mode correlations

The dielectric spectroscopy probes the dynamics of polymeric systems by measuring the complex permittivity

$\varepsilon(\omega)$, which is related to the correlation function $C_{\rm tot}(t)$ of the total polarization $\mathbf{P}_{\rm tot}(t)$ by the following relations:

$$\frac{\varepsilon(\omega)-\varepsilon_\infty}{\Delta\varepsilon}=-\mathcal{F}\left[\frac{\partial}{\partial t}C_{\rm tot}\right](\omega)=1-i\omega\mathcal{F}[C_{\rm tot}](\omega), \quad (37)$$

where ε_∞ is the permittivity due to the electronic polarization (i.e., not orientational), $\Delta\varepsilon$ is the overall orientational dielectric strength, $\mathcal{F}$ denotes the Fourier transform, and

$$C_{\rm tot}(t)=\frac{\langle\mathbf{P}_{\rm tot}(t)\cdot\mathbf{P}_{\rm tot}(0)\rangle}{\langle\mathbf{P}_{\rm tot}(0)\cdot\mathbf{P}_{\rm tot}(0)\rangle}. \quad (38)$$

We are interested in type-A polymers (according to the definition of Stockmayer[41]), i.e., linear polymers possessing a nonzero dipole component which is parallel to the chain backbone. In such polymers the dielectric experiments revealed the existence of various types of relaxation processes:[90] a ''normal-mode'' (α'-) relaxation related to the overall dipole $\mathbf{P}_\parallel(t)$ parallel to the chain backbone, probing the reorientation of the end–to–end vector, and the so-called ''segmental'' (α-) relaxation, related to the overall perpendicular dipole $\mathbf{P}_\perp(t)$, probing shorter length and time scales. The total polarization of a type-A polymer is written as

$$\begin{aligned}\mathbf{P}_{\rm tot}(t)&=\mathbf{P}_\parallel(t)+\mathbf{P}_\perp(t)\\&=\sum_{n=1}^{N}\left(\mu_\parallel\sum_{m=1}^{M-1}\mathbf{b}_{m,n}+\mu_\perp\sum_{m=2}^{M-1}\mathbf{t}_{m,n}\right).\end{aligned} \quad (39)$$

The average value of the static polarization for the two components is

$$\begin{aligned}\langle\mathbf{P}_\parallel(0)\cdot\mathbf{P}_\parallel(0)\rangle&=(\mu_\parallel)^2R_{\rm ee}^2/b^2,\\\langle\mathbf{P}_\perp(0)\cdot\mathbf{P}_\perp(0)\rangle&=(\mu_\perp)^2T_\perp^2.\end{aligned} \quad (40)$$

Equation (39) neglects the possible collective character of the dielectric relaxation. This follows from well-known experimental evidences that in most polymers, e.g., polyisoprene, the dipole moment is small and the intermolecular and intramolecular dipole–dipole interactions are negligible.[40]

In the present model the parallel and the transverse components of the permanent dipole associated to each monomeric unit were set to $\mu_\parallel=1$ and $\mu_\perp=1.5$, respectively. The ratio corresponds to *cis* polyisoprene.[40] The average modulus of the transverse dipole attached to each monomer is $\langle(p_\perp)^2\rangle=2(\mu_\perp)^2(1+\cos\hat{\theta})$ [see Eq. (11)] with $\cos\hat{\theta}=0.173$ at $T=1.0$, $P=2.0$, and a small dependence on the thermodynamic state. If the transverse dipole moment is well defined, one expects $\langle\mathbf{P}_\parallel(0)\cdot\mathbf{P}_\perp(0)\rangle=0$. For all the investigated thermodynamic states it is found

$$\frac{\langle\mathbf{P}_\parallel(0)\cdot\mathbf{P}_\perp(0)\rangle}{\sqrt{\langle P_\perp^2\rangle\langle P_\parallel^2\rangle}}=0.016\pm0.48. \quad (41)$$

We are now in a position to derive $C_{\rm tot}(t)$ from Eqs. (38) and (39). $C_{\rm tot}(t)$ exhibits the same scaling features of the other correlation functions (see Fig. 7). Having defined $\tau_{\rm tot}$ by Eq. (25) one finds $\tau_{\rm tot}/\tau_{\rm ee}\simeq\tau_{\rm tot}/\overline{\tau}=(2.6\pm0.3)\times10^{-1}$ (Fig. 8). The ratio reflects the non-negligible weight of the fast motion of $\mathbf{P}_\perp(t)$. It is worth noting that $\tau_{\rm tot}$ is comparable with the mean bond rotational correlation time $\tau_{\rm avg}$ (see Fig. 8).

In most experimental[60,90–92] and numerical studies,[47] the correlation between the parallel and the perpendicular polarization is neglected, i.e.,

$$\langle\mathbf{P}_\parallel(t)\cdot\mathbf{P}_\perp(0)\rangle=\langle\mathbf{P}_\parallel(0)\cdot\mathbf{P}_\perp(t)\rangle=0. \quad (42)$$

The assumption is motivated by the different time scales of $\mathbf{P}_\parallel(t)$ and $\mathbf{P}_\perp(t)$. The normal-mode relaxation time, related to the end–to–end relaxation time $\tau_{\rm ee}$, increases with the monomer number M, $\tau_{\rm ee}\propto M^2$ for oligomers, and $\tau_{\rm ee}\propto M^{3.4}$ for entangled systems.[30,60,93] On the contrary, the segmental relaxation time, related to $\tau_\perp$, depends much less on M, and is almost constant for entangled systems.

If the decoupling between $\mathbf{P}_\parallel(t)$ and $\mathbf{P}_\perp(t)$ is safe for high polymers, it becomes questionable for oligomers since the related time scales $\tau_{\rm ee}$ and $\tau_\perp$ are closer. In the present system $\tau_\perp/\tau_{\rm ee}\simeq\tau_\perp/\overline{\tau}=0.0283\pm0.0016$, close to the ratio $\tau_\perp/\tau_{\rm ee}\sim0.05$ found in poly-propylene-glycol) with $M=14$ at high T,[94] and the ratio $\tau_\perp/\tau_{\rm ee}=0.03\pm0.01$ for poly-cis-1,4-isoprene with $M\sim6-7$ by extrapolating data from higher molecular weight.[60,90] Neglecting the cross terms between the parallel and perpendicular components leads to the approximated total polarization correlation function given by the sum of two independent correlation functions, related to the parallel and the perpendicular polarizations

$$C_{\rm tot}(t)\simeq C_{\rm tot}^*(t)=a_\parallel C_{\rm ee}(t)+a_\perp C_\perp(t), \quad (43)$$

where $a_\parallel$ and $a_\perp$ are the relative dielectric strengths

$$a_\parallel=\frac{\Delta\varepsilon_\parallel}{\Delta\varepsilon_\parallel+\Delta\varepsilon_\perp}=\frac{(\mu_\parallel)^2R_{\rm ee}^2}{(\mu_\parallel)^2R_{\rm ee}^2+(\mu_\perp)^2T_\perp^2b^2}, \quad (44)$$

$$a_\perp=\frac{\Delta\varepsilon_\perp}{\Delta\varepsilon_\parallel+\Delta\varepsilon_\perp}=\frac{(\mu_\perp)^2T_\perp^2b^2}{(\mu_\parallel)^2R_{\rm ee}^2+(\mu_\perp)^2T_\perp^2b^2}. \quad (45)$$

Equation (43) expresses the dielectric relaxation as a weighted sum of two independent terms pertaining to well-defined dynamical processes, the reorientation of the end–to–end, and the ''segmental'' vectors. The strength ratio is

$$\frac{a_\parallel}{a_\perp}=\frac{(\mu_\parallel)^2R_{\rm ee}^2}{(\mu_\perp)^2T_\perp^2b^2}. \quad (46)$$

According to Fig. 2(a) the ratio between the normal and the segmental strengths decreases by increasing the density. Similar effects are reported by experiments[90,95] and simulations.[96]

To assess the approximation given by Eq. (43), $C_{\rm tot}(t)$ and $C_{\rm tot}^*(t)$ are compared in Fig. 12 for $T=0.7$ and $P=2.0$. The situation is analogous for the other (P,T) points. The agreement between $C_{\rm tot}(t)$ and $C_{\rm tot}^*(t)$ is fairly good at short and long times, but decreases at intermediate times, evidencing some degree of cross-correlation between the normal and the segmental motion. The discrepancy raises at the time scale t^* of the cage restructuring, reaches its maximum at $t\sim\tau_3\simeq\tau_{\rm ee}/9$, then it vanishes at $t\gg\tau_{\rm ee}$. τ_3 is the decay time of the third Rouse mode of the chain, to be defined in a more

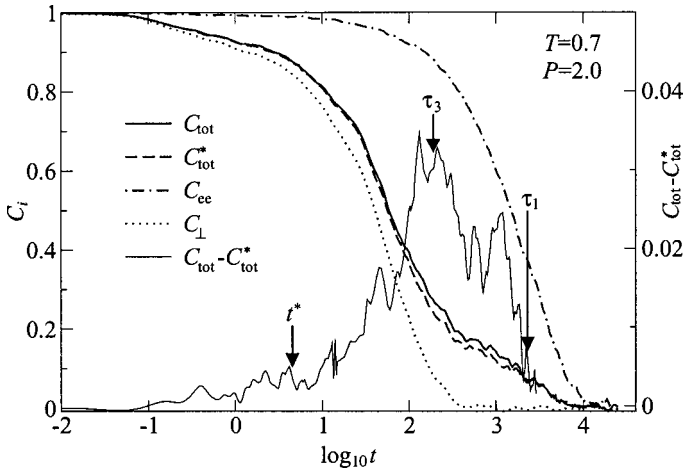

FIG. 12. Comparison between C_{tot}, C^*_{tot}, C_{ee}, $C_\perp$ (left axis), and $C_{tot}-C^*_{tot}$ (right axis) for $T=0.7$ and $P=2.0$.

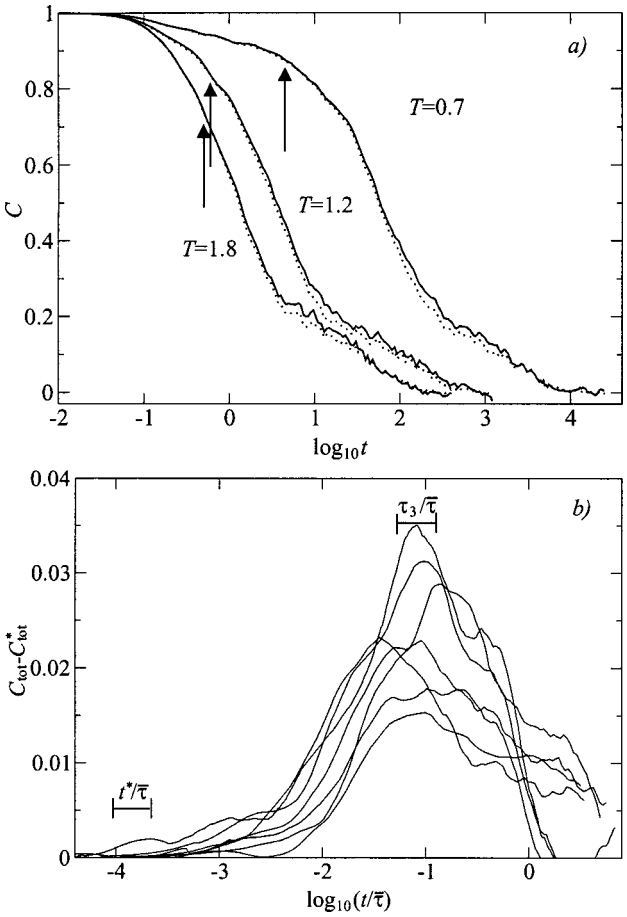

FIG. 13. (a) Representative plots of the correlation functions $C_{tot}(t)$ (solid lines) and $C^*_{tot}(t)$ (dotted lines) for the temperatures $T=0.7$, 1.2, and 1.8 and $P=2.0$; the arrows mark the time t^* where the nongaussian parameter α_2 reaches its maximum value for each temperature. (b) Comparison between the scaled functions $C_{tot}(t/\bar{\tau})-C^*_{tot}(t/\bar{\tau})$ for all the temperatures on the isobar $P=2.0$.

precise way below. The scenario represented in Fig. 12 holds also at different temperatures and pressures. As an example, the isobar $P=2.0$ is shown in Fig. 13.

These findings are readily intepreted. At $t<t^*$ the motion occurs inside the cage, no correlations exist between the frozen overall chain conformation and the fast dynamics of the monomers, which is largely independent on their position along the chain (see Fig. 4). At $t>t^*$ the cage structure relaxes and the motion becomes collective, i.e., the correlations between the monomers are not negligible. The bond dynamics is dependent on the position along the chain (see Fig. 4). In this regime appreciable correlations between the parallel and the normal components of the polarization are expected. The build-up of the correlations at $t>t^*$ occurs in the presence of an antagonistic phenomenon, namely, the finite correlation times of the collective motions due to the ongoing deformation of the chain. The longest correlation times set the lifetime of the cross correlations between the different components of the polarization. The collective motions of the polymer chain are usually described in terms of M modes $\mathbf{X}_p(t)$ with $p=0,\ldots M-1$ which are expressed as linear combination of the positions of the M monomers.[34,35] The p-th mode involves roughly the collective motion of $M/(p+1)$ monomers during the deformation of the chain. According to the Rouse model, the p-th mode $\mathbf{X}_p(t)$ has exponential correlation function with decay time τ_p given by[34,35]

$$\tau_p=\frac{\tau_1}{p^2}. \tag{47}$$

The first mode has the longest correlation time $\tau_1\simeq\tau_{ee}\simeq\bar{\tau}$. For $t>t^*$ the cage restructuring allows the onset of correlations between the end–to–end vector $\mathbf{R}_{ee}$ and the transverse one $\mathbf{T}$. As time goes by, the increase of the correlation is slowed down by the decreasing number of correlated collective modes, and is finally inhibited when only a few of them survive. According to Fig. 12, the largest correlations are found for times comparable to τ_3. For longer times only two modes, $\mathbf{X}_1(t)$ and $\mathbf{X}_2(t)$, still survive. But $\mathbf{X}_2(t)$ does not contribute to $\mathbf{R}_{ee}$, and thus to $\mathbf{P}_\parallel(t)$, because[34,35]

$$\mathbf{P}_\parallel(t)=-4\frac{\mu_\parallel}{b}\sum_{p:\mathrm{odd}}\mathbf{X}_p(t). \tag{48}$$

The above results suggest that the usual assumption of neglecting the cross-correlation terms in the dipolar correlation function $C_{tot}(t)$ may be questioned at least for oligomeric systems, where the correlations between parallel and perpendicular motions are more important. Our results point out that the correlations are detectable even if $\tau_{ee}/\tau_\perp\simeq 35$. Thus, the analysis of the correlation function $C_{tot}(t)$, or of the permittivity $\varepsilon(\omega)$, could be misleading if a simple superposition of ''normal-mode'' and ''segmental'' processes is imposed. As an example, Fig. 14(a) shows the real (ε') and the imaginary (ε'') parts of the permittivity, as calculated by Eq. (37) via the Fourier transform of the data in Fig. 13(a). The characteristic two-peak structure for $\varepsilon''(\nu)$ appears: the peak at lower frequencies is related to ''normal-mode'' process $[C_{ee}(t)]$ and the one at higher frequencies to the ''segmental'' one $[C_\perp(t)]$. As it can be noted, the exact permittivity, i.e. the one evaluated by $C_{tot}(t)$, is characterized by broader

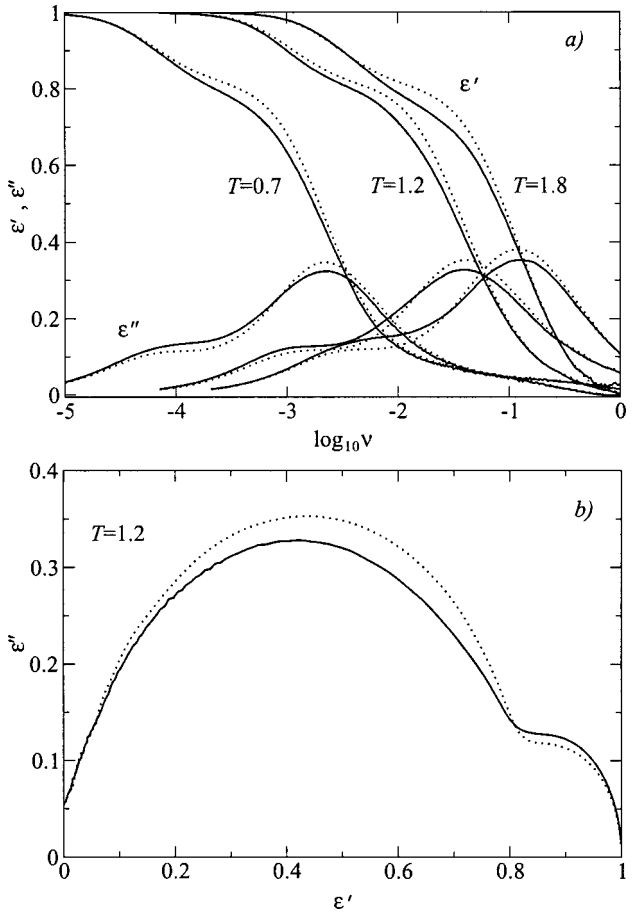

FIG. 14. (a) Representative plots of the complex permittivities as computed from the correlation functions $C_{\mathrm{tot}}(t)$ (solid lines) and $C^{*}_{\mathrm{tot}}(t)$ (dotted lines) for the temperatures $T=0.7$, 1.2, and 1.8 and $P=2.0$; (b) Cole–Cole plot of the complex permittivities of panel (a) for $T=1.2$.

peaks compared to the approximation derived by $C^{*}_{\mathrm{tot}}(t)$. Moreover, the exact permittivity of the normal mode is higher than the approximated one whereas the opposite occurs for the segmental mode. Such discrepancies are emphasized by plotting the imaginary versus the real part of the permittivity (the so-called Cole–Cole plot): each relaxation process is related to a semicircle, the low-frequency region, where the ''normal-mode'' is located, corresponds to high ε' values [see Fig. 14(b)].[93] The presence of non-negligible cross-correlations could explain the anomalous broadening of the relaxation peaks reported for the segmental and the normal-mode processes in some experiments on monodisperse polymeric melts[93] (see in particular Table II of Ref. 93). In fact, the analysis of the dielectric relaxation shape by means of a distribution of relaxation times has shown the overlap between the normal-mode and the segmental relaxation distributions for polymers with low molecular weight.[93]

H. Dielectric relaxation of type-A polymers: Lineshapes

The previous section pointed out that for chains with $M=10$ monomers the ''normal-mode'' and ''segmental'' processes give overlapping contributions to the total permittivity $\varepsilon(\omega)$ thus limiting the accuracy of the decoupling approximation, Eq. (42). The segmental process is almost independent of the molecular weight M, whereas the normal-mode component depends at least in a quadratic way. Then, on increasing M the two components yield two separate peaks of the permittivity $\varepsilon(\omega)$. The overlap of the peaks is made negligible when the chains are still poorly entangled, i.e., for $M\lesssim 40$.[36] In this short-chain regime changing the chain length simply shifts the normal-mode peak and leaves the segmental mode virtually unaffected, so that the master curves of each peak at $M=10$ provide information on their shape also for $M\lesssim 40$.

First, the normal-mode peak is considered. It is derived from Eq. (37) by replacing C_{tot} with the correlation function of the parallel polarization $\mathbf{P}_{\parallel}(t)$ which is proportional to $C_{\mathrm{ee}}(t)$ according to the relation

$$\langle \mathbf{P}_{\parallel}(0)\cdot\mathbf{P}_{\parallel}(t)\rangle = \left(\frac{\mu_{\parallel}R_{\mathrm{ee}}}{b}\right)^{2} C_{\mathrm{ee}}(t). \tag{49}$$

In the framework of the Rouse theory the correlation function of the end–to–end vector is expressed as[35]

$$C_{\mathrm{ee}}(t)=\sum_{p:\mathrm{odd}}^{M-1}\frac{8}{\pi p^{2}}\exp(-t/\tau_{p}). \tag{50}$$

According to Eq. (50) the decay is exponential at long times with the decay time of the first mode τ_1 and is stretched at shorter times due to the presence of additional modes. A typical comparison between the Rouse model and our results is provided by Fig. 15(a) which compares the master curve of C_{ee} at $P=2.0$ with Eq. (50) where τ_1 is adjusted to set the scale of Eq. (47). The agreement is quite good even if some deviation is seen for $0.01\leqslant t/\overline{\tau}\leqslant 1$ where the Rouse model does not fit accurately the stretched-exponential regime with stretching parameter $\beta=0.82$. The deviations are also seen in the plot of ε'' which is shown in Fig. 15(b). Finally, Fig. 15 confirms once more that the scaling procedure is more robust than the Rouse model. The disagreement may be partially ascribed to the well-known stretched-exponential decay of the correlation functions of the modes which is seen for bead-rod and bead-spring models of oligomeric systems.[45,51,97] This differs from the simple exponentials with decay times given by Eq. (47) which are predicted by the Rouse model. Another source of inadequacy is the fact the Rouse model poorly accounts for the fast motions localized on a few bonds and this limitation is important for the present model where the bond length is fixed. In fact, deviations from the Rouse model were reported by experiments carried out on different polymeric systems both at very high scattering vectors (short length scales) and high chain stiffness.[98–100]

Recently, Harnau *et al.*[101–103] developed the semiflexible chain model (SFCM), a modification of the Rouse model in order to represent the local chain stiffness effects. According to the SFCM, the mode relaxation times are given by

$$\tau_{p}^{\mathrm{SFCM}}=\frac{\tau_{1}}{p^{2}+a_{b}f(p)p^{4}}, \tag{51}$$

which differs from Eq. (47) for the p^4 term. $f(p)$ is a numerical factor increasing from $f(1)=0.25$ to the unit value for large p. The a_b parameter reads[104]

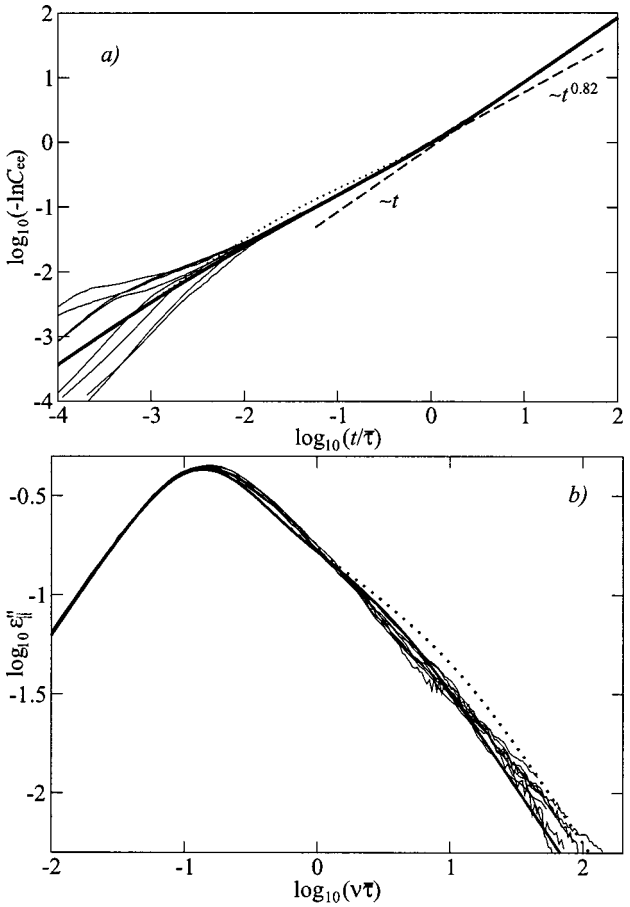

FIG. 15. (a) The master curve of the correlation function C_{ee} for all the temperatures on the isobar $P=2.0$ (thin lines). The dotted line is a fit with Eq. (50), the thick solid line is the best-fit of the SFCM model with $a_b=0.059\pm0.004$, and $\tau_1=1.15\pm0.04$. The exponents of the power-laws give the stretching parameters of C_{ee} at intermediate and long times and (b) the master curve of the dielectric permittivity $\varepsilon''_{\parallel}$ derived from the correlation functions of panel (a).

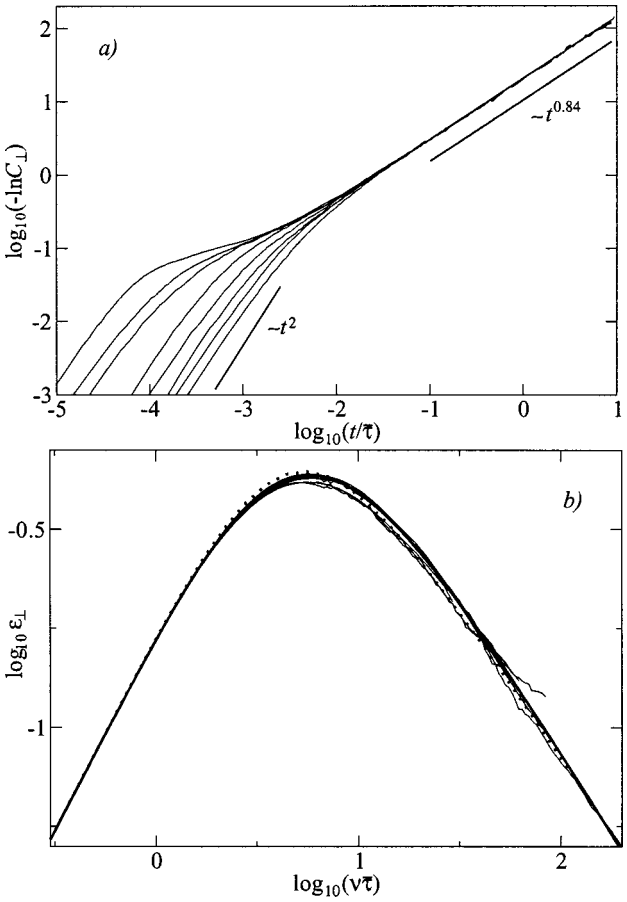

FIG. 16. (a) The master curve of the correlation function $C_{\perp}(t)$ for all the temperatures on the isobar $P=2.0$. The exponents of the power-laws give the stretching parameters of $C_{\perp}$ and (b) the master curve of the dielectric permittivity $\varepsilon''_{\perp}$ derived from the correlation functions of panel (a) (thin lines), the thick and dotted lines are fits with a Cole–Davidson function ($\beta_{CD}=0.767$) and by taking $C_{\perp}(t)$ to be a stretched exponential with $\beta_{KWW}=0.84$, respectively.

$$a_b=\left[\frac{\pi C_M}{2(M-1)}\right]^2, \tag{52}$$

where C_M is the characteristic ratio defined by Eq. (2). The a_b parameter is virtually temeperature-independent in that $a_b=0.056$ at $T=0.7$, $P=2.0$, and it changes to $a_b=0.064$ at $T=1.8$,$P=2.0$. We fitted the SFCM model to our master curves by adjusting τ_1 and a_b. The results are shown in Fig. 15(a) for $C_{ee}(t)$ and in Fig. 15(b) for ε''. SFCM improves the fit with the best-fit value $a_b=0.059\pm0.004$ over all the interval $10^{-2}\leqslant t/\bar{\tau}\leqslant 10^2$.

The shape of the peak of the permittivity $\varepsilon(\omega)$ due to the segmental relaxation is now considered. It is derived from Eq. (37) by replacing C_{tot} with the correlation function of the perpendicular polarization $\mathbf{P}_{\perp}(t)$ which is proportional to $C_{\perp}(t)$ according to the relation

$$\langle \mathbf{P}_{\perp}(0)\cdot\mathbf{P}_{\perp}(t)\rangle=(\mu_{\perp}T_{\perp})^2C_{\perp}(t). \tag{53}$$

Figure 16(a) presents the master curve of $C_{\perp}(t)$ at $P=2.0$. After the ballistic regime with Gaussian decay and a plateau-like region the decay is described by a stretched-exponential with $\beta=0.84$. The stretching is very close to that found for $C_{ee}(t)$ in the same time window [see Fig. 15(a)]. Figure 16(b) plots the corresponding ε'' which is fitted fairly well by the Fourier transformed stretched exponential with $\beta_{KWW}=0.84$ or with a Cole–Davidson function with $\beta_{CD}=0.767$, following the relationship found by Lindsey and Patterson for the shape parameters of the two functions.[105] The comparison with the Rouse model is not pursued further since the latter is not expected to describe with accuracy the fast decay of $C_{\perp}(t)$. The comparison with the SFCM model is more promising and is under current development.[87]

IV. CONCLUSIONS

Results of extensive MD simulations of a polymer melt have been presented. The thermal and the density effects on the statics and the dynamics have been investigated in wide temperature and pressure ranges.

In the explored thermodynamic region, a global time-temperature-pressure superposition principle (TTPSP) for both the translation and the rotational dynamics holds and a single scaling time $\bar{\tau}$ is found. $\bar{\tau}$ is very close to the correlation time of the end–to–end vector τ_{ee} and the diffusion time τ_{diff}. The scaling argument is more robust than the Rouse model and relies on neglecting at long times ($t>t^*$) the finer

details of the interactions between each monomer and its surroundings so that the motion is accounted for by average viscoelastic forces.

The thermodynamic states of the polymer model were well fitted by the phenomenological Tait equation of state. The dimensionless constant r_T which is derived by the best-fit parameters is found to be in the range of real polymers.

The isochronic α_τ and isobaric α_P expansivities were investigated. By examining the ratio $|\alpha_\tau|/\alpha_P$ between the isochronic and isobaric expansivities, one finds that the temperature is dominant when the dynamics is fast. If the relaxation slows down, the fluctuations of the free volume increase their role and become comparable to those of the thermal energy.

The MD simulations were used to model the dielectric relaxation of type-A polymers. The so called ''normal-mode'' relaxation has been related to the end–to–end vector self correlation function, while the ''segmental'' relaxation to the self correlation function of a vector built from units which are locally orthogonal to the chain backbone. For chains with $M=10$ monomers the normal and segmental modes overlap with appreciable cross-correlations which prevent one to consider them as being independent to each other. On increasing the chain length the two modes are well separated. For unentangled chains the master curve of the normal mode is well fitted by the semiflexible chain model,[101–103] a modification of the Rouse model developed in order to account for the local chain stiffness.

ACKNOWLEDGMENTS

M. Lucchesi is warmly thanked for several enlightening remarks and suggestions. The writers also thank G. Floudas for providing us his data, R. Casalini and M. Paluch for helpful discussions, and T. Voigtmann for some hints about the Fourier transform algorithm.

[1] C. A. Angell, Science **267**, 1924 (1995).
[2] F. H. Stillinger, Science **267**, 1935 (1995).
[3] P. G. Debenedetti and F. H. Stillinger, Nature (London) **410**, 259 (2001).
[4] C. A. Angell, K. L. Ngai, G. B. McKenna, P. F. McMillan, and S. W. Martin, J. Appl. Phys. **88**, 3113 (2000).
[5] D. Turnbull and M. Cohen, J. Chem. Phys. **52**, 3038 (1970).
[6] G. Adam and J. H. Gibbs, J. Chem. Phys. **43**, 139 (1965).
[7] W. Götze and L. Sjögren, Rep. Prog. Phys. **55**, 242 (1992).
[8] G. Williams, Trans. Faraday Soc. **60**, 1548 (1964).
[9] H. Sasabe and S. Saito, J. Polym. Sci. [A1] **6**, 1401 (1968).
[10] G. P. Johari and E. Whalley, Faraday Symp. Chem. Soc. **6**, 23 (1973).
[11] K. U. Schug, H. E. King, and R. Böhmer, J. Chem. Phys. **109**, 1472 (1998).
[12] M. Paluch, A. Patkowski, and E. Fischer, Phys. Rev. Lett. **85**, 2140 (2000).
[13] M. Paluch, R. Casalini, S. Hensel-Bielowka, and C. M. Roland, J. Chem. Phys. **116**, 9839 (2002).
[14] H. Leyser, A. Schulte, W. Doster, and W. Petry, Phys. Rev. E **51**, 5899 (1995).
[15] S. Corezzi, S. Capaccioli, R. Casalini, D. Fioretto, M. Paluch, and P. A. Rolla, Chem. Phys. Lett. **320**, 113 (2000).
[16] R. Casalini, S. Capaccioli, M. Lucchesi, P. A. Rolla, and S. Corezzi, Phys. Rev. E **63**, 031 207 (2001).
[17] R. Casalini, S. Capaccioli, M. Lucchesi, P. A. Rolla, M. Paluch, S. Corezzi, and D. Fioretto, Phys. Rev. E **64**, 041 504 (2001).
[18] R. Casalini, M. Paluch, J. J. Fontanella, and C. M. Roland, J. Chem. Phys. **117**, 4901 (2002).
[19] J. T. Bendler, J. J. Fontanella, and M. F. Shlesinger, Phys. Rev. Lett. **87**, 195 503 (2001).
[20] I. Avramov, J. Non-Cryst. Solids **262**, 258 (2000).
[21] P. B. Macedo and T. A. Litovitz, J. Chem. Phys. **42**, 245 (1965).
[22] T. Pakula, J. Mol. Liq. **86**, 109 (2000).
[23] M. L. Ferrer, C. Lavrence, B. G. Demirjian, D. Kivelson, C. Alba-Simonesco, and G. Tarjus, J. Chem. Phys. **109**, 8010 (1998).
[24] K. L. Ngai, L. Bao, A. F. Yee, and C. L. Soles, Phys. Rev. Lett. **87**, 215 901 (2001).
[25] M. Paluch, R. Casalini, and M. Roland, Phys. Rev. B **66**, 092 202 (2002).
[26] M. Paluch, C. M. Roland, and A. Best, J. Chem. Phys. **117**, 1188 (2002).
[27] M. Paluch, C. M. Roland, J. Gapinski, and A. Patkowski, J. Chem. Phys. **118**, 3177 (2003).
[28] M. Naoki, H. Endou, and K. Matsumoto, J. Phys. Chem. **91**, 4169 (1987).
[29] G. Floudas and T. Reisinger, J. Chem. Phys. **111**, 5201 (1999).
[30] G. Floudas, C. Gravalides, T. Reisinger, and G. Wegner, J. Chem. Phys. **111**, 9847 (1999).
[31] S. P. Andersson and O. Andersson, Macromolecules **31**, 2999 (1998).
[32] S. W. Smith, B. D. Freeman, and C. H. Hall, Macromolecules **30**, 2052 (1997).
[33] F. Müller Plathe, Chem. Phys. Carbon **3**, 754 (2002).
[34] P. E. Rouse, J. Chem. Phys. **21**, 1272 (1953).
[35] M. Doi and S. F. Edwards, *The Theory of Polymer Dynamics* (Clarendon Press, Oxford, 1986).
[36] K. Kremer and G. S. Grest, J. Chem. Phys. **92**, 5057 (1990).
[37] K. Binder, J. Bashnagel, and W. Paul, Prog. Polym. Sci. **28**, 115 (2003).
[38] C. Bennemann, W. Paul, J. Bashnagel, and K. Binder, J. Phys.: Condens. Matter **11**, 2179 (1999).
[39] Y. N. Kaznessis, D. A. Hill, and E. J. Maginn, J. Chem. Phys. **111**, 1325 (1999).
[40] K. Adachi and T. Kotaka, Macromolecules **18**, 466 (1985).
[41] W. Stockmayer, Pure Appl. Chem. **15**, 539 (1967).
[42] M. P. Allen and D. J. Tildesley, *Computer Simulation of Liquids* (Clarendon Press, Oxford, 1987).
[43] S. Nosé, Prog. Theor. Phys. Suppl. **103**, 1 (1991).
[44] H. C. Andersen, J. Chem. Phys. **72**, 2374 (1980).
[45] C. Bennemann, J. Bashnagel, W. Paul, and K. Binder, Comput. Theor. Polym. Sci. **9**, 217 (1999).
[46] M. Guenza, Macromolecules **35**, 2714 (2002).
[47] M. Fixman, J. Chem. Phys. **69**, 1538 (1978).
[48] C. F. Abrams and K. Kremer, J. Chem. Phys. **115**, 2776 (2001).
[49] C. F. Abrams and K. Kremer, J. Chem. Phys. **116**, 3162 (2002).
[50] C. De Michele and D. Leporini, Phys. Rev. E **63**, 036 701 (2001).
[51] A. Barbieri, D. Molin, and D. Leporini (unpublished).
[52] C. De Michele and D. Leporini, Phys. Rev. E **63**, 036 702 (2001).
[53] S. Kämmerer, W. Kob, and R. Schilling, Phys. Rev. E **56**, 5450 (1997).
[54] P. T. L. Fabbian and F. Sciortino, J. Non-Cryst. Solids **235–237**, 325 (1998).
[55] A. Barbieri, G. Gorini, and D. Leporini (unpublished).
[56] H. Takeuchi and R. J. Roe, J. Chem. Phys. **94**, 7446 (1991).
[57] N. E. Moe and M. D. Ediger, Polymer **37**, 1787 (1996).
[58] R. D. de la Batie, F. Laupetre, and L. Monnerie, Macromolecules **22**, 122 (1989).
[59] S. H. Chong and M. Fuchs, Phys. Rev. Lett. **88**, 185 702 (2002).
[60] D. Boese and F. Kremer, Macromolecules **23**, 829 (1990).
[61] P. D. Hyde and M. D. Ediger, Macromolecules **22**, 1510 (1989).
[62] R. Zorn, D. Richter, B. Farago, B. Frick, F. Kremer, U. Krist, and L. J. Fetters, Physica B **180**, 534 (1992).
[63] J. Kanetakis, G. Fytas, F. Kremer, and T. Pakula, Macromolecules **25**, 3484 (1992).
[64] F. Alvarez, J. Colmenero, J. Kanetakis, and G. Fytas, Phys. Rev. B **49**, 14996 (1994).
[65] D. J. Plazek, E. Schlosser, A. Schonhals, and K. L. Ngai, J. Chem. Phys. **98**, 6488 (1993).
[66] D. Richter, B. Frick, and B. Farago, Phys. Rev. Lett. **61**, 2465 (1988).
[67] D. Richter, R. Zorn, B. Farago, B. Frick, and L. Fetters, Phys. Rev. Lett. **68**, 71 (1992).
[68] M. Aichele and J. Baschnagel, Eur. Phys. J. E **5**, 245 (2001).
[69] M. Paluch, S. Pawlus, and C. M. Roland, Macromolecules **35**, 7338 (2002).
[70] C. M. Roland and R. Casalini, J. Chem. Phys. **119**, 1838 (2003).
[71] B. J. Punchard and D. B. Adolf, J. Chem. Phys. **117**, 7774 (2002).
[72] R. K. Bharadwaj and R. H. Boyd, J. Chem. Phys. **114**, 5061 (2001).
[73] M. H. Cohen and D. Turnbull, J. Chem. Phys. **31**, 1164 (1959).
[74] K. L. Ngai, J. Non-Cryst. Solids **275**, 7 (2000).
[75] C. Bennemann, W. Paul, K. Binder, and B. Dünweg, Phys. Rev. E **57**, 843 (1998).

[76] N. Kärger, T. Vardag, and H.-D. Lüdermann, J. Chem. Phys. **93**, 3437 (1990).
[77] R. L. Cook, H. E. King Jr., C. A. Herbst, and D. R. Herschbech, J. Chem. Phys. **100**, 5178 (1994).
[78] G. Fytas, T. Dorfmüller, and C. H. Wang, J. Chem. Phys. **87**, 5041 (1983).
[79] M. Paluch, S. Hensel-Bielówka, and J. Ziolo, J. Chem. Phys. **110**, 10978 (1999).
[80] J. Köplinger, G. Kasper, and S. Hunklinger, J. Chem. Phys. **113**, 4701 (2000).
[81] G. Floudas, G. Fytas, T. Reisinger, and G. Wegner, J. Chem. Phys. **111**, 9129 (1999).
[82] M. Paluch, C. M. Roland, and S. Pawlus, J. Chem. Phys. **116**, 10932 (2002).
[83] D. Prevosto, M. Lucchesi, S. Capaccioli, R. Casalini, and P. A. Rolla, Phys. Rev. B **67**, 174 202 (2003).
[84] D. W. VanKrevelen, *Properties of Polymers* (Elsevier Science, Amsterdam, 1997).
[85] R. Simha, P. S. Wilson, and O. Olabisi, Kolloid-Z. **251**, 402 (1973).
[86] S. Corezzi, M. Lucchesi, P. A. Rolla, S. Capaccioli, G. Gallone, and M. Paluch, Philos. Mag. B **79**, 1953 (1999).
[87] A. Barbieri, S. Capaccioli, and D. Leporini (unpublished).
[88] C. M. Roland, M. Paluch, T. Pakula, and R. Casalini, Philos. Mag. B (submitted).
[89] C. M. Roland, R. Casalini, P. Santangelo, M. Sekula, J. Ziolo, and M. Paluch, Macromolecules **36**, 4954 (2003).
[90] K. Adachi and T. Kotaka, Prog. Polym. Sci. **18**, 585 (1993).
[91] D. Boese, F. Kremer, and L. J. Fetters, Polymer **31**, 1831 (1990).
[92] T. Kotaka and K. Adachi, Macromol. Symp. **79**, 125 (1994).
[93] Y. Imanishi, K. Adachi, and T. Kotaka, J. Chem. Phys. **89**, 7585 (1988).
[94] A. Schonhals and E. Schlosser, Phys. Scr., T **49**, 233 (1993).
[95] K. L. Ngai, A. Schonhals, and E. Schlosser, Macromolecules **25**, 4915 (1992).
[96] Y. N. Kaznessis, D. A. Hill, and E. J. Maginn, Macromolecules **32**, 1284 (1999).
[97] J. T. Padding and W. J. Briels, J. Chem. Phys. **117**, 925 (2002).
[98] A. Maconnachie, P. Vasudevan, and G. Allen, Polymer **19**, 33 (1978).
[99] G. Allen, J. S. Higghins, A. Maconnachie, and R. E. Ghosh, J. Chem. Soc., Faraday Trans. **78**, 2117 (1982).
[100] J. S. Higghins, Br. Polym. J. **19**, 103 (1987).
[101] L. Harnau, R. G. Winkler, and P. Reineker, J. Chem. Phys. **101**, 8119 (1994).
[102] L. Harnau, R. G. Winkler, and P. Reineker, J. Chem. Phys. **102**, 7750 (1995).
[103] L. Harnau, R. G. Winkler, and P. Reineker, J. Chem. Phys. **106**, 2469 (1997).
[104] V. A. Harmandaris, V. G. Mavrantzas, D. N. Theodorou, M. Kroger, J. Ramirez, H. C. Ottinger, and D. Vlassopoulos, Macromolecules **36**, 1376 (2003).
[105] C. Lindsey and G. D. Patterson, J. Chem. Phys. **73**, 3348 (1980).
[106] Y. X. Yi and P. Zoller, J. Polymer Sci., Part B: Polym. Phys. **31**, 779 (1983).
[107] V. K. Sachdev, U. Yahsi, and R. K. Jain, J. Polym. Sci., Part B: Polym. Phys. **36**, 841 (1998).
[108] M. Schmidt, M. Olsson, and F. H. J. Maurer, J. Chem. Phys. **112**, 11095 (2000).